FINAL REPORT

INVESTMENT CASTING SHELL CRACKING

By

Von Richards

January 2000-May 2003.

University of Missouri, Rolla

Award Number: DE-FC07-00ID13845

Acknowledgement: This material is based upon work supported by the U.S. Department of Energy under Award No. DE-FC07-00ID13845.

Primary Contractor:	Tri-State University, Angola Indiana
Subcontractor:	University of Missouri-Rolla, Rolla, Missouri
Other Partners:	Steel Founders' Society of America Mercury Marine Propeller Division Conbraco Industries Precision Metalsmiths Hitchiner Manufacturing
Contacts:	Principal Investigator Von L. Richards University of Missouri – Rolla Department of Metallurgical Engineering 1870 Miner Circle Rolla, MO 65409-0001 573-341-4730 vonlr@umr.edu
Project Team:	DOE-HQ contact: Harvey Wang Industry Contact: Raymond Monroe, Steel Founders' Society of America Project mentor: Bob Trimberger, DOE Idaho Contract Specialist: Marshall Garr, DOE Idaho

Final Technical Report

INVESTMENT CASTING SHELL CRACKING

Executive Summary

This project made a significant contribution to the understanding of the investment casting shell cracking problem. The effects of wax properties on the occurrence of shell cracking were demonstrated and can be measured. The properties measured include coefficient of thermal expansion, heating rate and crystallinity of the structure.

The important features of production molds and materials properties have been indicated by case study analysis and fractography of low strength test bars. It was found that stress risers in shell cavity design were important and that typical critical flaws were either oversize particles or large pores just behind the prime coat. It was also found that the true effect of fugitive polymer fibers was not permeability increase, but rather a toughening mechanism due to crack deflection.

I. Comparison of Goals and Accomplishments

Goal	Accomplishments
Upgrade in-process testing	• AN ANOVA study was completed to show the benefits of four point bend as opposed to three point bend testing and to show the effects sample preparation technique on shell material testing. • Demonstrated that cristallinity and relaxation effects occur in pattern wax and influence the stress applied to shells in the autoclave process. • Developed a non-contact method to measure wax expansion that can be done with feedback hotplate, thermocouple readout and computer interfaced digital camera.
Reduce shell cracking scrap	• Demonstrated the effect of wax reclamation process on thermal expansion behavior of pattern wax. This correlated with increased shell cracking scrap at the participating foundry.
Evaluation of shell material bench tests	• Evaluated three-point and four-point flexure tests and sample preparation techniques for shell strength samples • Measured toughness, elastic modulus, and coefficient of thermal expansion for shell materials.
Evaluate correlation of shell process parameters,	• Demonstrated that toughness and not permeability improvement was the effect that improved autoclave

bench test, and shell manufacturing performance	performance when fugitive polymer fibers were added to the shell formulations. • Demonstrated that low strength shells were limited by build flaws. Most common flaws were: 1. -large particles at the interface between prime coat and first back-up coat 2. -delamination or pores at the interface between prime coat and first back-up layer.

II. Introduction:

Shell cracking is an age-old problem in investment casting. The objective of this program is to develop an understanding of the problem of shell cracking in the investment casting manufacturing environment and developing laboratory tests for mold materials that can be used as control tests to characterize shells in the production environment. This final report reviews five key areas in the investment-casting program: four-point bend testing, wax thermal expansion, sonic modulus testing, fracture toughness testing and permeability of the shells. Each of these key tasks is presented as separate sections; the student participants under the supervision of P.I Dr.Von Richards performed these tests.

The conceptual framework for these tasks is based on the concepts of elastic stress analysis and fracture. Essentially, the wax expansion during mold de-waxing imposes on stress on shell since thermal expansion of shell is lower than that of wax. The stress on the shell depends on the elastic response superposition required to constrain the free strain of the wax. This results in a high stress at the intersections of long surfaces of the shell with the ends other surfaces. The tensile properties of the ceramic bars depend on the size and geometry of the existing flaws. As a consequence we need to characterize the elastic response of the shell, the strength distribution of the shell (flaw population) and fracture toughness of shell material. The thermal expansion of shell is also a factor to be considered in rigorous elastic modeling of shell-wax interaction.

III. FOUR-POINT BEND TESTING TO CHARACTERIZE THE STRENGTH OF CERAMIC MOLD SHELLS

Dr. Von L. Richards

Student Participants: Craig Erford, James Sturgeon, Teck-Seng"Chris"Tan, Deepak R, Ginger Conin, Phil Jackson and Sony Mascreen

III.(i) Introduction:

The tensile properties of the ceramic bars depends on the size and geometry of the existing flaws, so there is a considerable scatter in the values of strength determined by a tensile, bending or fatigue test. Ceramic parts produced with the same materials and using similar methods fail at very different loads. In order to design structural parts using ceramics, the probability that a flaw present will cause failure to occur at any given stress must be known. The Weibull distribution and Weibull modulus provides one statistical approach to designing with ceramics.

Samples from all of the participating foundries were tested. The three-point bend test is the prevalent method of determining the strengths of shells in industry but the four-point bend test is thought to give more accurate results than the three-point method and was used in all strength measurements. A four-point bend method has been developed for testing the properties of ceramic mold shells. The four-point method subjects the tensile portion of the sample to a uniform stress over a specified region. By comparison, the stress varies over the test length of three-point modulus of rupture test, reaching the calculated value at only one point. A fully equalized fixture was built and tested following the concepts of error reduction in ceramic testing proposed by F.I. Baratta, (Baratta,1982) for technical ceramics. Sample preparation is critical for these tests. Therefore a wax pattern was developed to minimize the preparation damage and stress concentrations on the tensile side of the test bar. Although shell cracking usually occurs during de-waxing, the flaw population of the ceramic is preserved through firing

III.(ii) Designing the Test Mold:

In developing the testing procedure we looked at some case studies of shell cracking at participant foundries. It appears that most frequently the cracking began as a tensile fracture of the hot face (or primary coat) surface in a highly stressed region. Therefore we concluded that the tensile strength of the face side of the shell might be most important.

The test article was designed taking into account some of the sources of error in flexure testing of ceramics discussed by Baratta (Baratta, 1982). In that reference Baratta takes into account the following sources of error:

Nonlinear stress distribution

Initial curvature of the specimen

Anticlastic curvature

Large deflections

Wedging stress

Tangency point shift

Neglect of corner radii effects on area moment of inertia

Contact stress.

As with any design, there were some compromises, particularly in making the test article producible by the participating casters and in attempting to utilize equipment which would already be available in steel foundries having other molding processes included in their suite of manufacturing processes. The effect of non-linearity of stress distribution was limited by use of L/d ratios of nine-to-ten depending on the participant's process. L and d are defined in figure 1b.

Initial specimen curvature was typically of the order of radius to thickness greater than 100, so this effect is negligible. The effect of anticlastic curvature should be negligible since the range of width to thickness for the bars was four to six. The effects of

large deflections were limited by the relatively low strength of the bars being tested, less than 0.5 percent at the L/d ratio used.

The error due to wedging stress was considered negligible again due to the small deflection before fracture even though the a/d ratios ranged between 1.2 and 1.4. “a” is the distance from the loading point to the support point, and “a” and “d” are defined in figure 1b.

Test bar mold was designed with about a 0.16-in radius while typical specimen thickness was .25 inches to 0.4 inches. This would lead to about eight percent systematic error in the specimen strength reported. However, the radius was included based on input from the participating casters that a tighter radius would lead to build-up of the face coat in the edges of the tensile face of the test bar. Our test design included using the tensile surface of the flexure sample and the edges of that surface generated by the shell build-up process. The existing methods at some of the participants involved either building-up a sheet of shell material on a flat paddle and releasing it by impact, then testing the material that does not fracture, or building-up a shell on a flat wax article and sanding or sawing the edges. In the former case we felt we would have proof tested and eliminated lower strength material containing critical flaws causing fracture at low stress. In the latter case we attempted this method, but found that the degree of “proof testing” which occurred in the sanding or sawing step depended on the manual skills of the technician and that we were inducing fine cracks and flaws due to particle “pull-out” on the edge of the tensile side of the test article.

Contact stress was one area in which we violated the recommended criterion due to equipment space limitations, with a contact radius of only about .25 inches where 1.5 inches would have been calculated from the recommendations given by Baratta. The only ameliorating factor here is that our breaking stress to elastic modulus ratio was probably lower than the 10^{-3} value used by Baratta.

We initially specified groups of fifteen to twenty samples based on the frequently cited Weibull modulus of about twenty in the investment casting literature. As will become apparent later, this sample size was too small because the Weibull modulus of production materials is below this by a statistically significant amount. Having a fully articulated fixture compensated the effects of specimen twist.

III.(iii) Experimental Procedure:

The ceramic test bars used in this procedure were made with the tensile side against the wax. Each participating foundry was given the test bar mold. The foundries injected the mold with their wax (Figure 2). The mold then went through each foundry's slurry process. In some cases the areas marked by the arrows were wiped wet, but in other cases they were inaccessible during coating so they were sawn off afterwards. The tensile bar has a flattened "U" shape to it. Both unfired and fired bars were to be tested by the four-point bend method. For each test, about fifteen to twenty bars would be prepared. The test bars would be cut on the compression side (rough side) (Figure 3). Nothing was done to the tensile (smooth) side (Figure 4). Using the diamond saw, the bar was cut on the compression side to remove the legs of the "U". A 260-grit diamond-polishing wheel was used to obtain the desired flat surface. A very flat surface was desirable. This meant sanding some of the bars with 220-grit sandpaper. The sandpaper was placed on glass to ensure a flat sanding. Once the specimens were ready, they were put in the oven at 150°C for three hours. The three hours in the oven was only for the previously fired bars. (Unfired bars had a different procedure, which is mentioned below.)

When the samples were cool enough, they were weighed. The length and thickness were measured in millimeters and recorded. They were then broken on the four-point bend apparatus (Figure 5). The load to break the bar was recorded in Newtons. If any bars broke at or outside the four-point bend points, the data was considered suspect and left out of the statistical analysis.

Unfired bars were also tested using the same preparation as the fired bars. About 15 bars were used per trial. The difference begins after being cut with the saw. Once the unfired bars were cut, they were not sanded. This was because the unfired bars cut much more easily. They gave a very flat surface to work with. Length and thickness in millimeters was once again recorded. Due to the bars being wet for this test, the weight was not recorded. The bars were placed in 95°C water for one hour. The bars were then tested in the 4-point bend apparatus. To do this, the hot bar was extracted using tongs. It was then placed in the 4-point bend apparatus. The load to break the bar was recorded in Newtons. Testing of unfired test bars helps us simulate the actual conditions of the

ceramic material in an autoclave. Heating the test bar in water to boiling temperature melts the wax on the surface of the bar (the same happens in an autoclave). This test helps us draw conclusions on the effect of polymers on the strength of shells.

III.(iv) Results:

The results in three areas will be covered:

1. Comparison of cut coupons to the mold coupons from the design discussed above
2. Four-point bend as a measure of process drift over time
3. Three- point bend versus four-point bend

Comparison of cut bar versus the proposed test article design is shown in table I. The cut coupon has a lower Weibull modulus but a higher mean strength. Considering a normal distribution the cut bar shows a higher standard deviation of strength values.

The comparison of three-point bend results to four point bend results at two foundries is summarized in table II. Although the statistical significance may be questionable, the trend toward giving a higher nominal strength value with three-point bend is evident.

The process drift over time at one of the participating foundries is shown as a Weibull plot for three different sampling times in figure 6. These are four-point results using the proposed test bar design. The Weibull modulus was greatly different at each of these samplings: 4.8, 2.6, and 11.7. Weibull Modulus for each of the participating foundries was calculated. The graphs for each of the participating foundries are as shown in Figures7 to 9. Figure 10 shows the comparison of weibull plot with fibrous shell samples from participant B.

III.(v) Discussion of Results:

The cut coupon has a higher mean strength than the molded bar from (the designed test bar) and a broader distribution of test values. During sanding to obtain straight edges on the test bars cut from flat coupons, several of the bars broke. Thus the weaker bars from the sample population were eliminated, giving a false high mean strength. At the same time, the sawing and sanding introduced flaws in the edge of the test pieces on the tensile side, which superimposed another flaw distribution in addition to the flaws introduced in the shell-making process. This would give rise to the broadened breaking stress

distribution compared to the proposed test article design. The molded bars did have clean-up diamond saw cutting and sanding on them to generate a uniform and measurable thickness, but this was all done on the compression side of the flexure bar, while the tension side and its edges were generated by the wax pattern. The explanation for the trend to higher mean strengths in the three point bend test as compared to the four point bend test is not statistically significant, but does seem logical considering that a smaller region of the sample is exposed to the maximum tensile stress in the three point bend test than in the four point test. Thus, the probability of encountering a flaw from the large size tail of the population distribution is lessened when three-point bend is used.

Figure 10 shows the comparison of weibull moduli of non-fibrous polymer shell sample to the fibrous shell sample. The weibull modulus is slightly higher for the fibrous samples (5.27) when compared with non-fibrous samples from the same foundry (4.71).

The Weibull moduli are lower than commonly reported from samples prepared by impact removal from a waxed paddle. The Weibull moduli are lower than the value initially used to select the sample size, which leads to some additional inaccuracy. As indicated by figure 11 (from Baratta), at the 90% confidence level the characteristic strength should be determined within plus or minus ten percent, but the Weibull modulus will only be known within plus or minus thirty percent at these levels with only twenty to twenty two samples. However, the process drift is clearly bigger than the error bar on the measurement, so that the characteristic strength and Weibull modulus do represent real changes in the process.

III.(vi) Conclusions and Recommendations:

The conclusions we can draw from this study to date are:

1. The molded test bar is more representative of the shell building process than a sanded or sawed bar prepared from a flat sample
2. The four-point bend method should be more representative of the weakest link in the shell structure, but this has not been proven to a statistically significant extent.
3. Weibull moduli of test lots can represent the variation of shell strength due to process variations.

Recommendation:

Use a test bar that has the tension surface and the edges of the tension surface generated by the prime coat and shell build, rather than prime coat with the edges generated by abrasion or sawing.

III.(v) References

1. *Francis I. Baratta, Requirements for Flexure testing of Brittle Materials, AMMRC TR 82-20, Army Materials and Mechanics Research Center, Watertown, MA, 1982.*

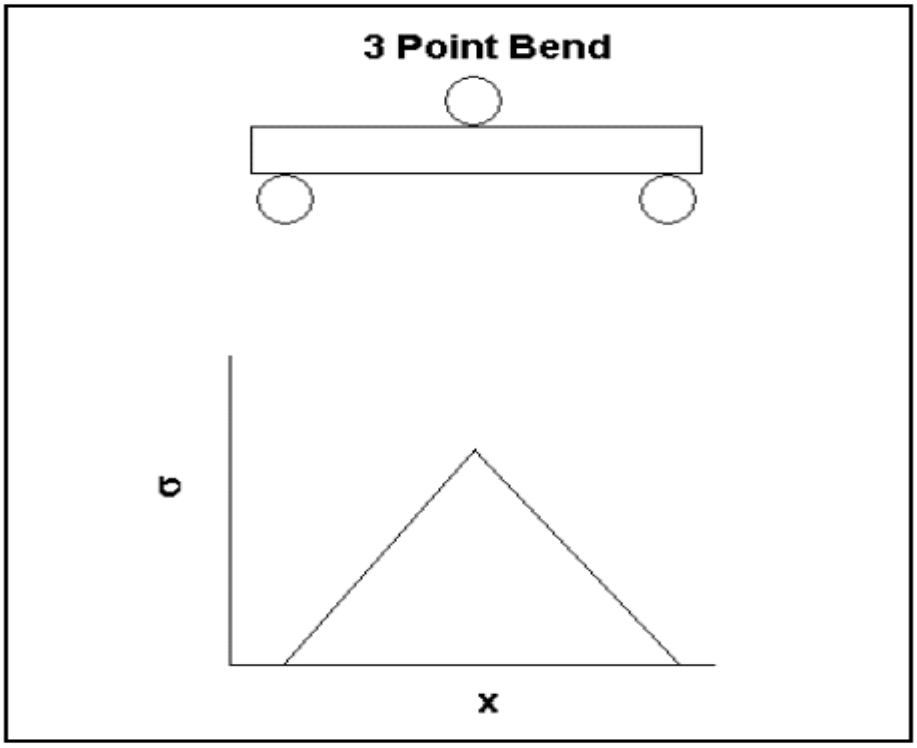

Figure 1 a. Stress Distribution in Three Point Bend Testing

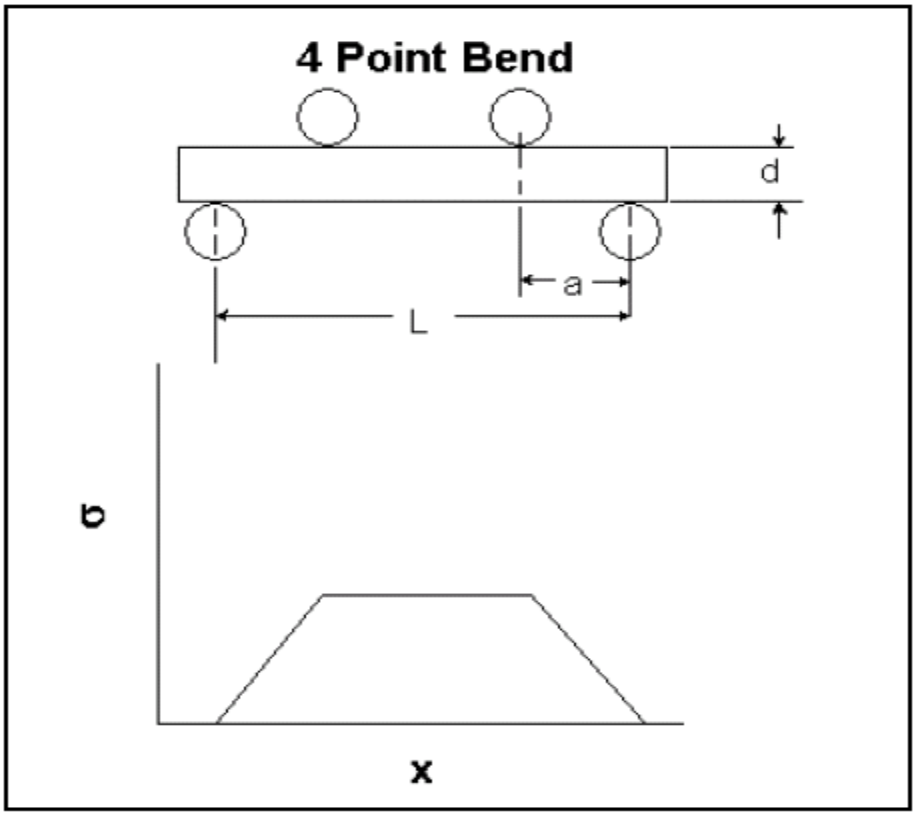

Figure 1b. Stress Distribution in Four Point Bend Testing

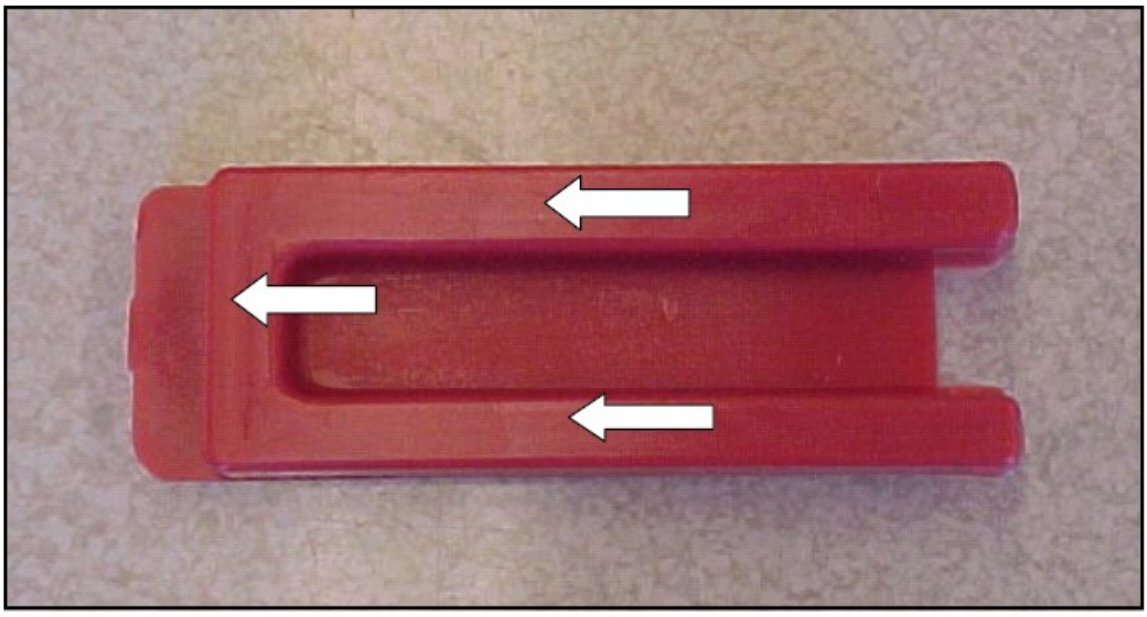

Figure 2: Test Bar Mold, the Injected Wax Portion to be Dipped in Slurry. Arrows Indicate Optional Wet Strike-Off Flats.

Figure 3: Compression Side of Test Bar Showing Sawn and Sanded Areas

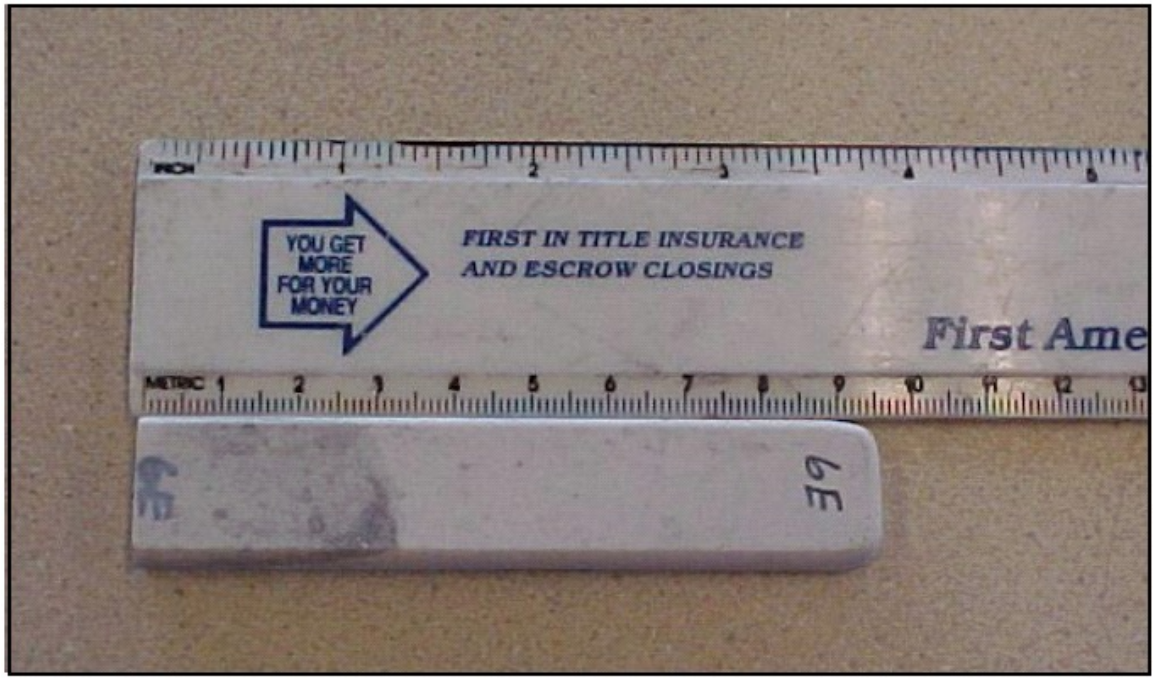

Figure 4: Tensile Side of Test Bar

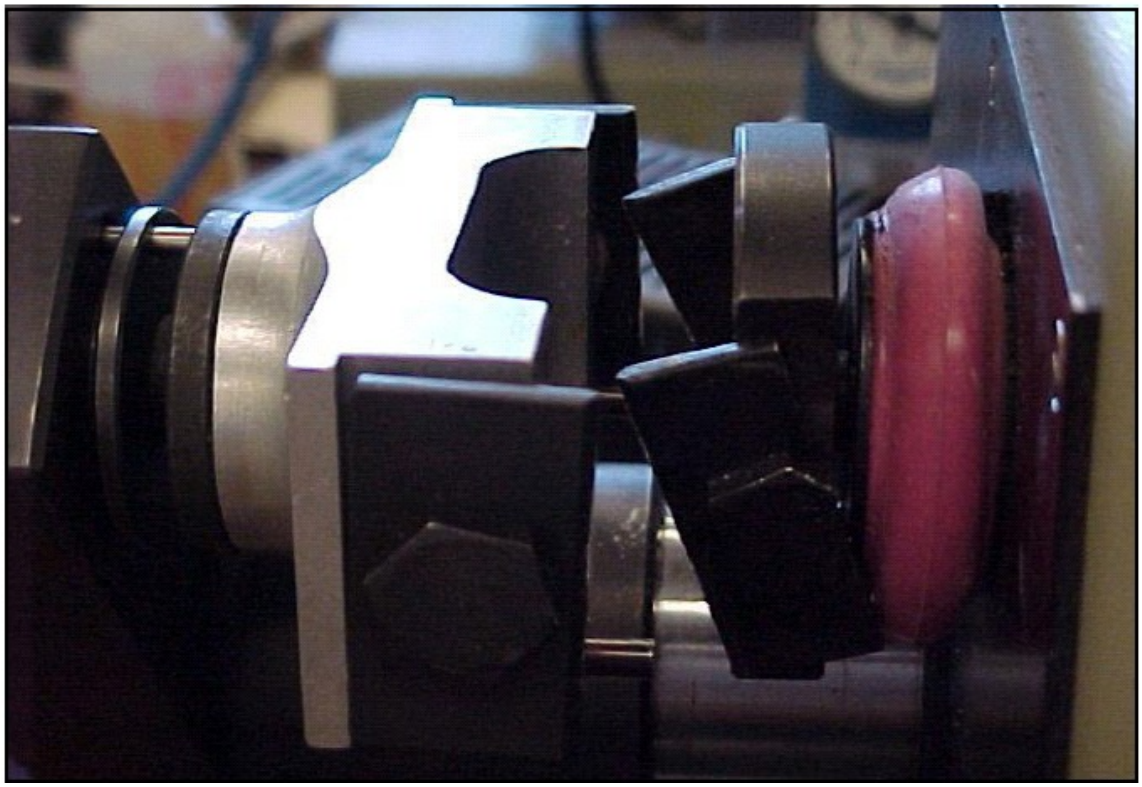

Figure 5: Four-Point Bend Apparatus

Table I. Comparison of Cut Coupons to Designed Test Bar (Molded)

	Weibull Modulus	Mean Strength	Standard Deviation (normal distribution)
Cut Coupon	5.77	2.14 MPa	0.525 MPa
Designed test article (molded bar)	9.98	1.75 MPa	0.175 MPa

Table II. Comparison of Three-Point Bend to Four Point Bend

Participating Foundry	Method	Mean Strength (MPa)	Standard Deviation (MPa)
B	3-point	1.26	0.20
B	4-point	1.22	0.24
C	3-point	3.32	0.59
C	4-point	3.15	0.49

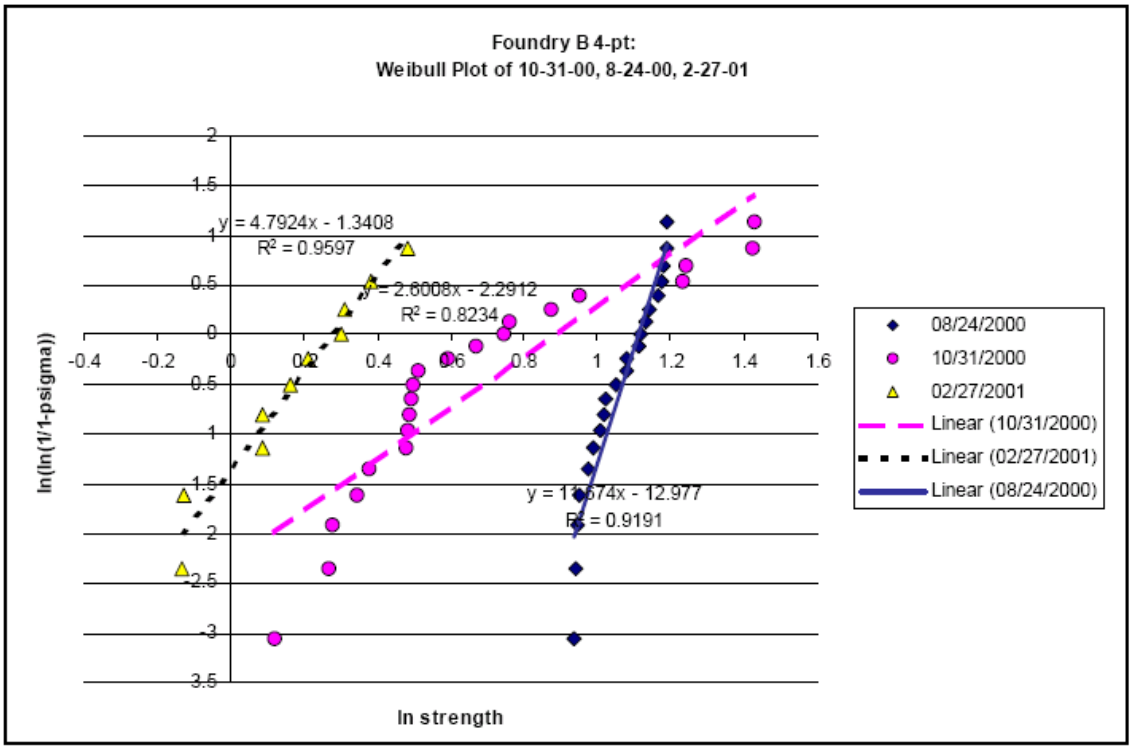

Figure 6: Process Variation over Time at One Participating Foundry (Note that some of this was due to intentional changes by the foundry.)

Unfired Shell-Foundry C.

Date of Receipt:06/05/01
Date of Test: 10/15/01
Weibull Modulus 6.98
Regression Line:
-0.02939+6.98492 ln (strength)

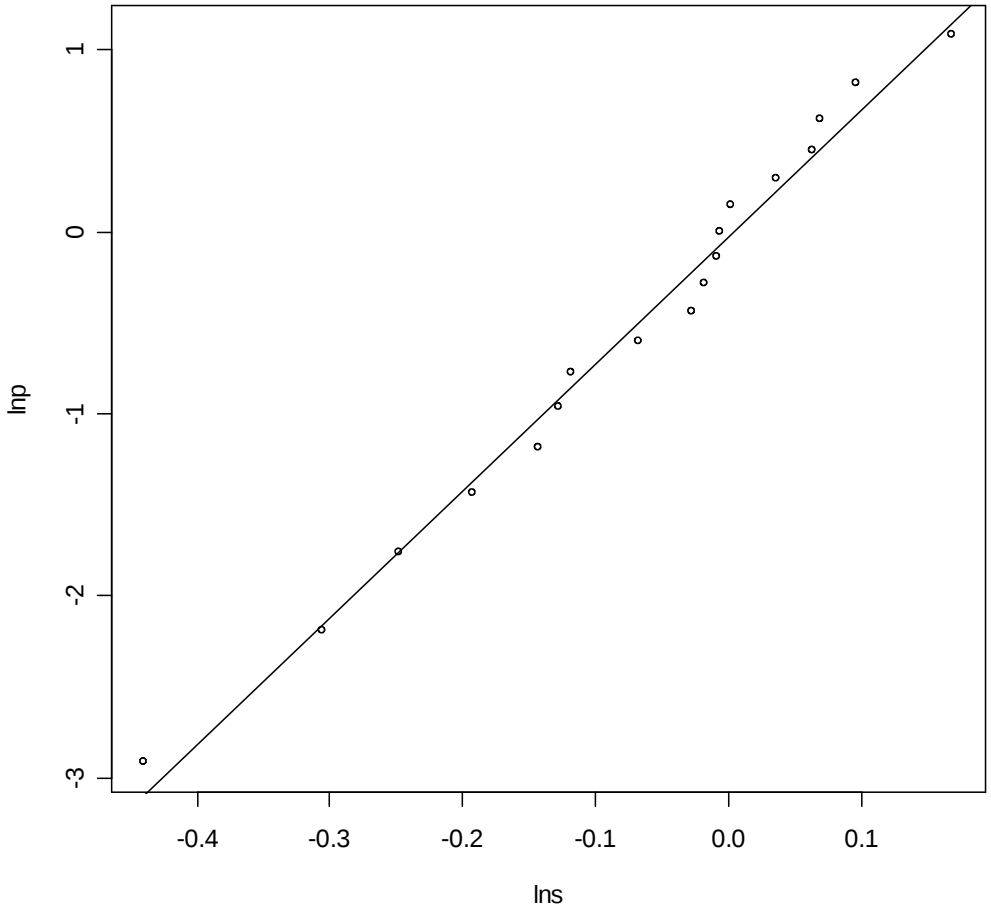

Figure 7: Plot of Cumulative Probability Versus Fracture Strength

Fired Shell-Foundry C
Firing Temperature: 1300F
Molds are dark in appearance
Date of Receipt: 06/06/01
Date of Test: 12/06/01
Weibull Modulus= 1.559

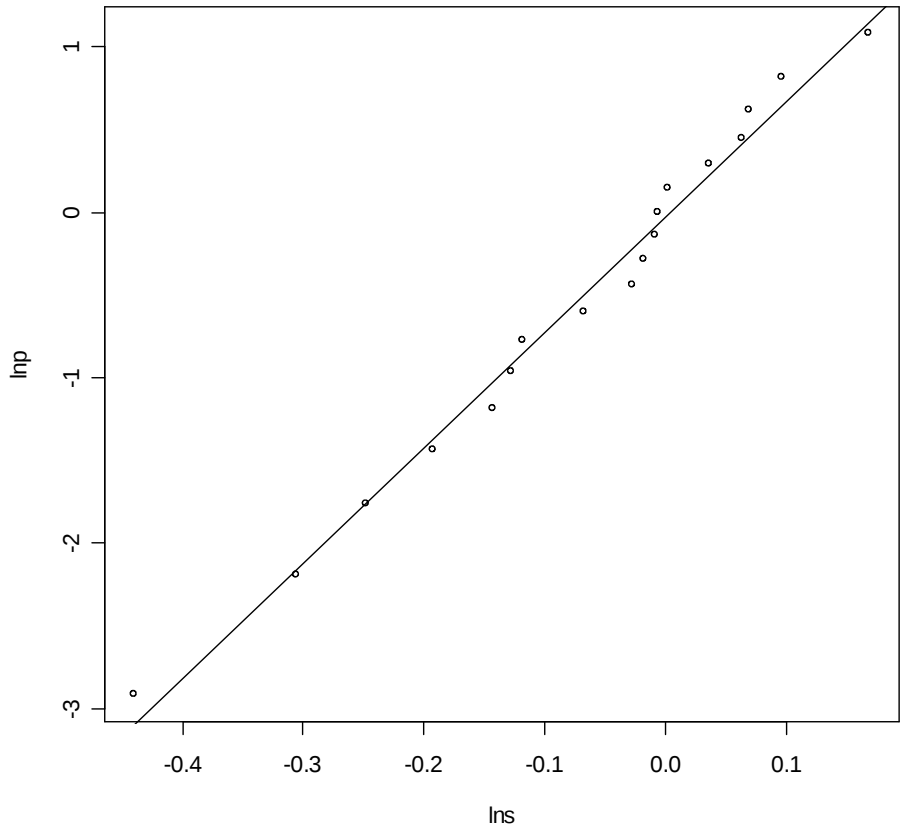

Figure 8: Plot of Cumulative Probability Versus Fracture Strength

Fired Shell- Foundry A
Date of Receipt:06/05/01
Date of Test: 10/15/01
Weibull Modulus: 5.1598
Regression line:
1.1289+5.1598ln(strength)

R-squared= .9502

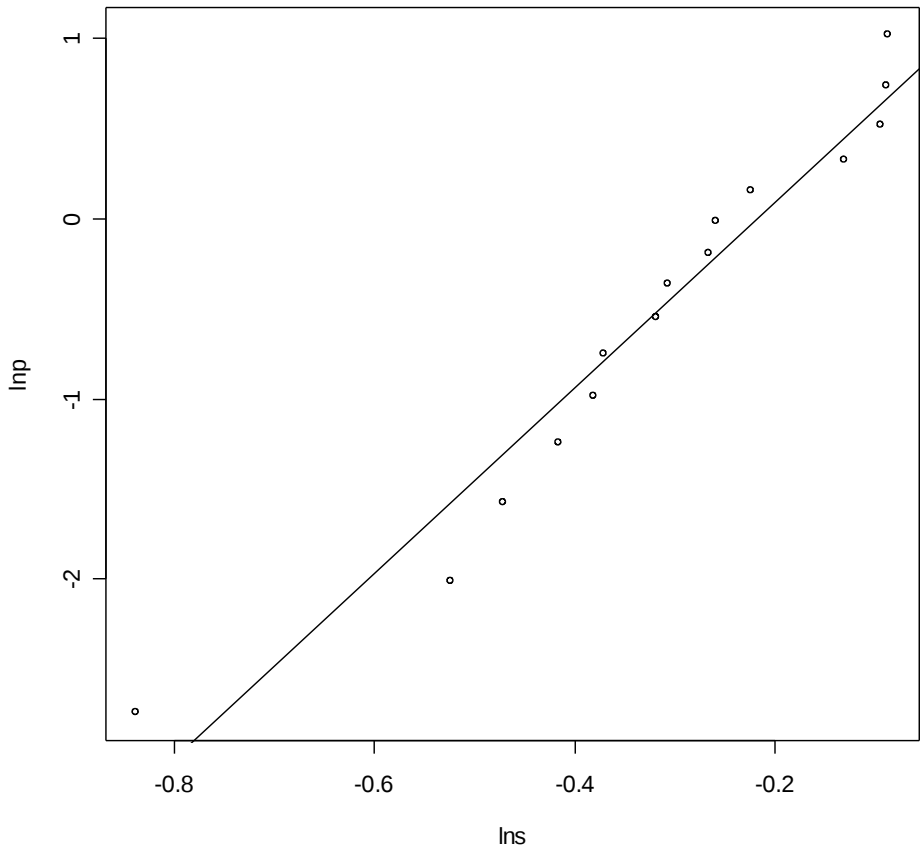

Figure 9: Plot of Cumulative Probability Versus Fracture Strength

Unfired Shell- Foundry A
Date of Receipt:06/05/0
Date of Test: 12/06/01
Weibull Modulus: 6.019

Regression Line: 20886+6.01975ln(strength)
R-squared: 0.9779

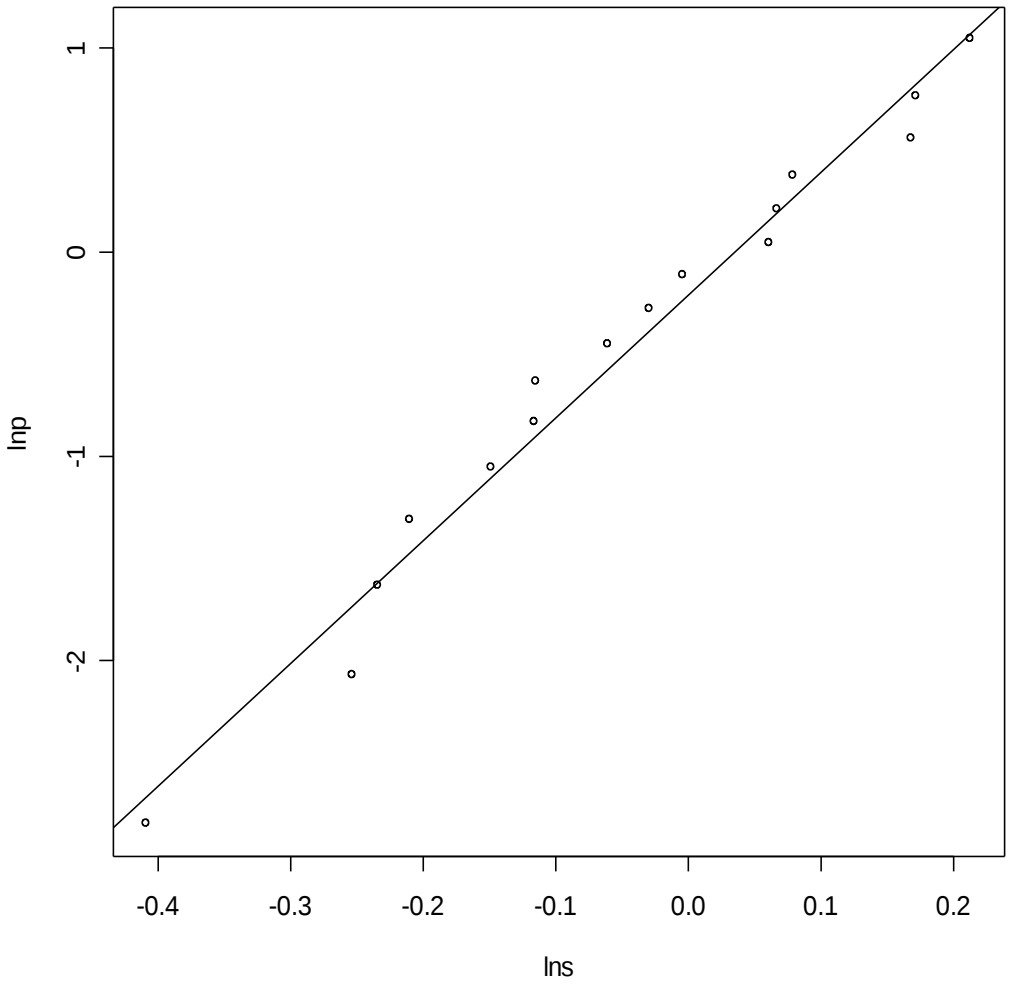

Figure 10: Plot of Cumulative Probability Versus Fracture Strength

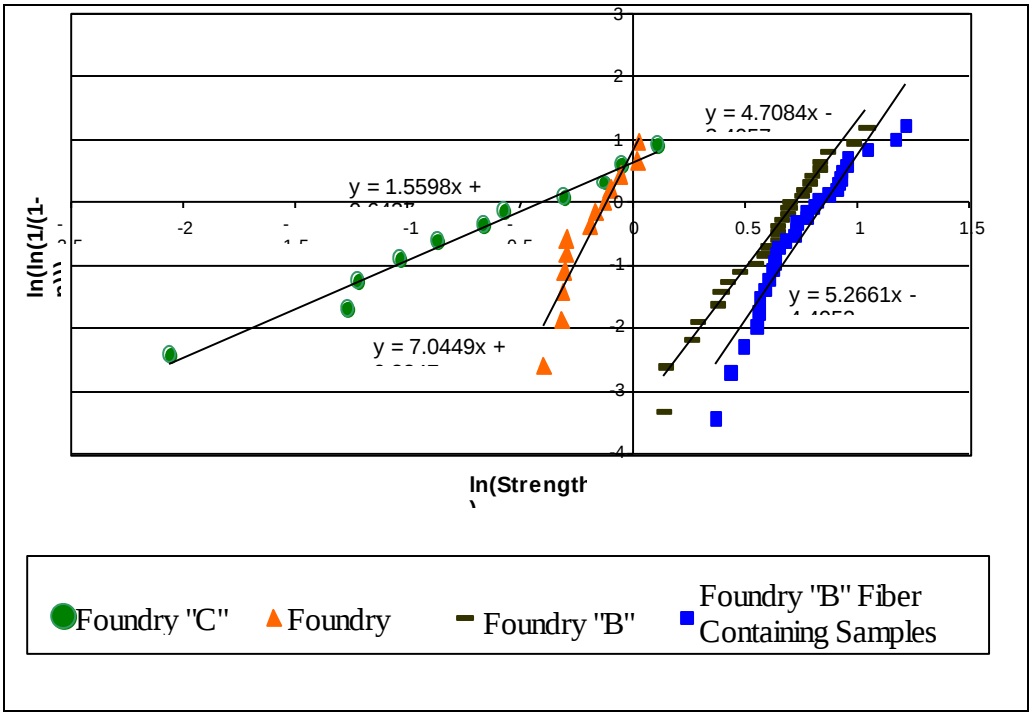

Figure 10: Comparison of Weibull Plots of Participating Foundries

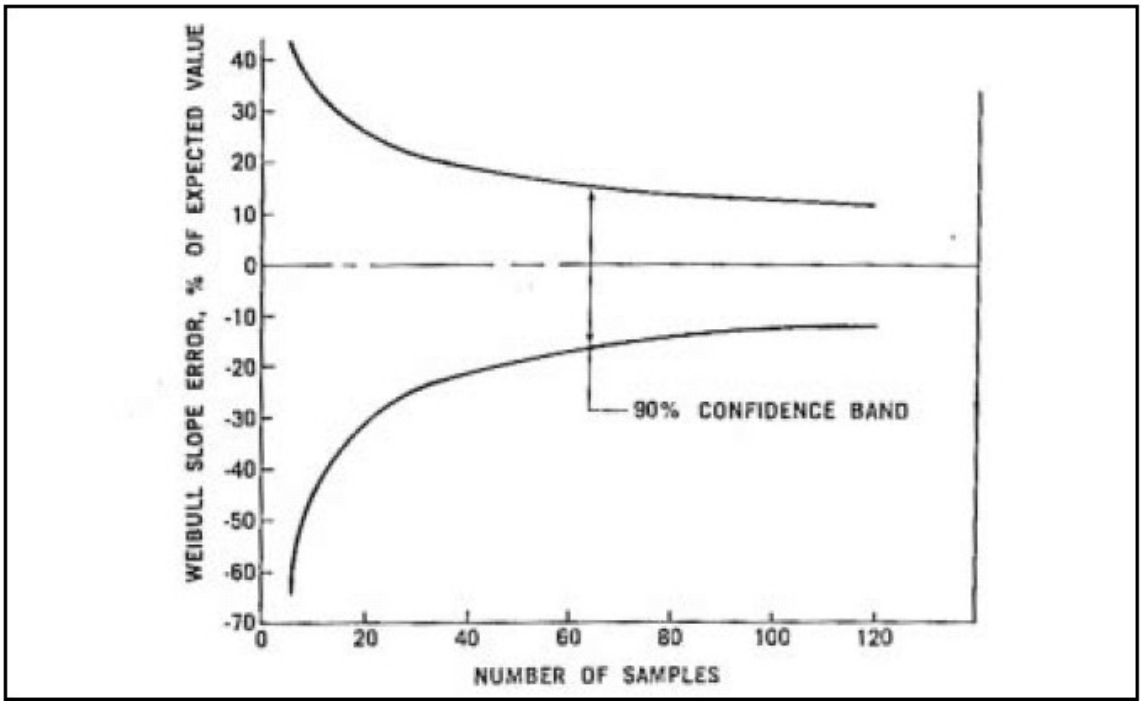

Figure 11A . Error in Weibull Parameter Determination based on Number of Samples (from Baratta, 1982)

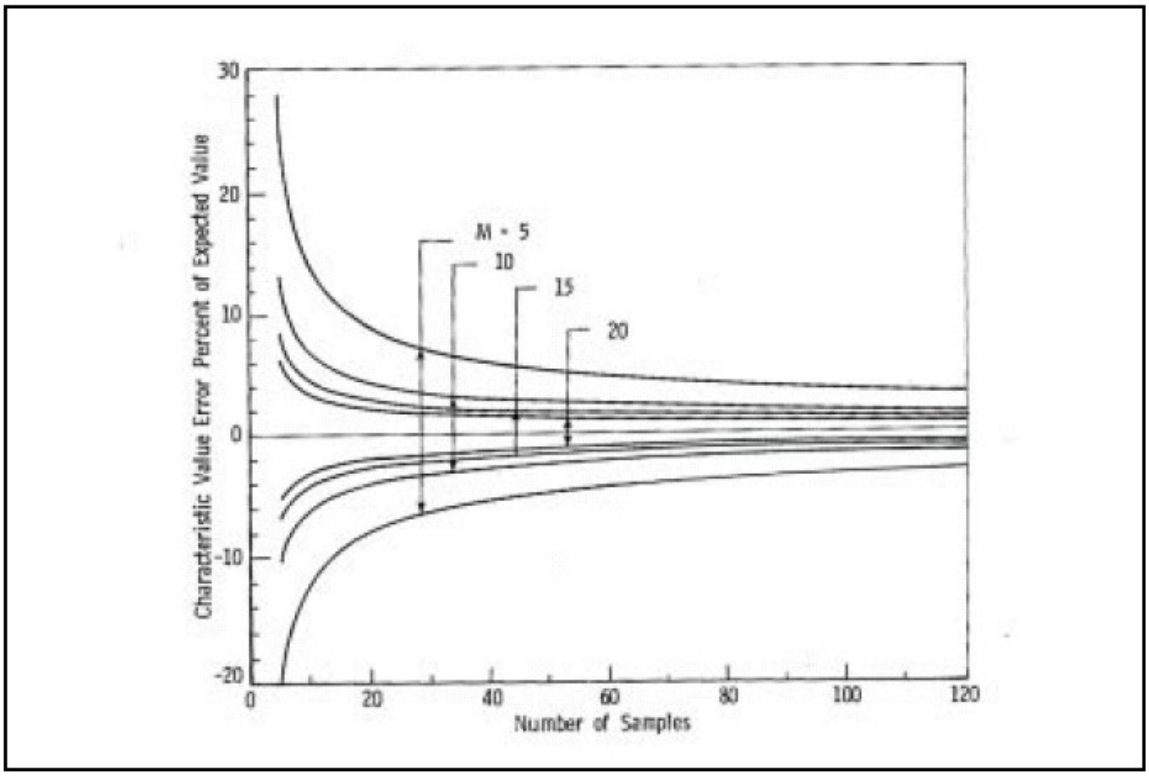

Figure 11B . Error in Characteristic Strength Value based on Weibull Slope and Sample Size (Baratta, 1982)

IV. FRACTURE TOUGHNESS OF INVESTMENT CASTING SHELLS USING FRACTOGRAPHY

Von L. Richards, Ph.D.
University of Missouri at Rolla
And
Student Research Participant; Sony Mascreen, James Sturgeon

IV.(i) Background

The purpose of fractography is to analyze the fracture features and relate these features to find the causes of fracture. While conducting the four-point bend test on ceramic mold shell samples, used in investment casting, we found some samples had exceedingly low strengths that looked like outliers in the Weibull analysis. Our participating foundries were interested in examining these low strength ceramic shell samples. Fractographic analysis was used to find the cause of failure of these samples. Results showed shell build flaws were responsible for some of the failures; therefore we decided to find fracture toughness of these broken samples using fractography. This method is an unconventional way of finding the fracture toughness. The determination of plane-strain fracture toughness, K_{Ic}, is important in understanding the material

characteristics of investment casting shells. Once the value of K_{Ic} is calculated we can more thoroughly understand the fracture mechanics of the shell itself. Using microscopic analysis we are able to find the critical flaw that induced the fracture, and the fracture toughness can be calculated by using Griffith's crack theory.

Additionally, we explored artificially induced flaws using a knoop indenter in conjunction with the four-point bend test to get fracture toughness. Here a crack is induced in the sample using a knoop indenter. The breaking strength is obtained by the four-point bend test and the growth and depth of crack is observed using fractography. The two methods are compared in the paper.

IV.(ii). Introduction

The study of fracture mechanics and fracture toughness is an important aspect in describing a material's resistance to fracture. This differentiates between the material's intrinsic resistances to crack extension, which can be considered more or less severe depending on parameters like processing, handling etc. We know that in brittle fracture, presence of a crack-like defect leads to unstable rapid failure when the stresses at the crack tip will exceed a critical value. This critical value called K_{IC}, the plane strain fracture toughness, is the property of a material that gives its inherent resistance of that material to failure in the presence of a crack-like defect. The relation connecting the fracture toughness and the crack length is given by *(Ref 1)*

$$K_{Ic}=Y\sigma\,(\pi a)^{1/2} \quad \text{.....(1)}$$

Where: Y is a geometric constant

σ is the stress applied to cause crack propagation

a is the length of an edge crack

The tensile stress σ is obtained from the four-point bend testing of the molded test bars. The procedure for this is given in detail in the next section. The geometric factor Y is dependent on the specimen and crack geometry. For a semi elliptical surface crack with major plane of crack perpendicular to the applied tensile stress, the stress intensity factor is given by (*Ref 2)*

$$K_I^2=1.21\pi a\,\sigma^2/Q \quad \text{.....(2)}$$

Where: Q is the flaw shape parameter.

Figure-1 shows flaw shape parameter Q, plotted against the crack-shape ratio a/2c. Here "c" is the width of the crack and σ_0 is the yield strength. In brittle materials yield strength is equal to the tensile strength, therefore σ/σ_0 =1. Using these we get the value of crack shape parameter and hence a more accurate fracture toughness value can be calculated.

This paper is a continuation of work done earlier in Tri-State University by the first author. This method used the Knoop hardness tester in an attempt to create a flaw that could be measured after fracture. The different indentation loads used are 44.15N, 58.86N, and 68.67N, the procedure for which is given later.

Fractography, a very useful and effective technique, has an important role in understanding the fracture strength and behavior of ceramics. We use fractography to identify the critical flaw that induces the fracture. Here we are looking into the inherent flaw in the samples that we have broken using four point bend apparatus to get the strength of the samples.

The eventual purpose of the work reported in this paper is to determine whether the reproducible features of the microstructure of shell material can be used to adjust the toughness. It is a further objective to determine if that toughness is less dependent on the random flaws than is the measured strength. Varying the toughness could then be used to make the shells more robust against the random flaws induced during shell build.

IV.(iii) Procedure

IV.(iii).a. Sample Preparation

The ceramic test bars used in this procedure were made with the tensile side against the wax. Each participating foundry was given the test bar mold. The foundries injected the mold with their wax. The mold then went through each foundry's slurry process. The tensile bar has a flattened "U" shape to it as shown in figure 2.

The test bar material was produced by participating foundries using the design described by Richards, et al (*Ref 3*). Fired bar material was used for the processes described here. The test bars would be cut on the compression side (rough side). Nothing was done to the tensile (smooth) side. Using the diamond saw, the bar was cut on the

compression side to remove the legs of the "U" until a flat specimen remained. A 260-grit diamond-polishing wheel was used to obtain the desired flat surface. Once the specimens were ready, they were heated in an oven at 150°C for three hours. Length and thickness were measured in millimeters and recorded. The samples were then broken on the four-point bend apparatus shown in figure 3.

IV.(iii).b. Four Point Bend Test

A four-point bend method has been developed earlier for testing the properties of ceramic mold shells (*Ref 3*). The bend testing method developed was based on the ASTM standard C1161-94, and the work of Baratta *(Ref 4)*. The four-point method subjects the tensile portion of the sample to a uniform stress over a specified region. A fully equalized fixture was built and tested following the concepts of error reduction in ceramic testing proposed by F.I. Baratta (*Ref 4*) for technical ceramics. The load to break the bar was recorded in Newtons. If any bars broke at or outside the four load points, the data was considered suspect and left out of the statistical analysis. Fractographic studies were done on the low strength bars obtained from the four-point bend test. Strength of the molded samples from each foundry was tested. Richards, et al, discussed the analysis of these test bars in detail *(Ref 3)*. The Weibull plots for the participating foundries are given in figure 5. These plots show the lots of bars tested contained multiple flaw distributions, so that fitting a single Weibull modulus to the data would be inappropriate.

IV.(iii).c. Indentation and Four Point Bend Test

The sample, which was to be tested using an induced flaw, was also prepared as above. A knoop indenter was used to induce the flaw and the indentation was made on the center of the tensile side of the sample. The long axis of the indenter was kept perpendicular to the applied tensile force. The loads used for the indentation were 44.15N, 58.86N, and 68.67N. The area that was indented was dyed using a Neopen J.A.P. - S.H.F. Penetrant, then the samples were dried at 150 ^{0}C for 3 hours. Afterward all the bars were broken on the four-point bend apparatus. The load to break the bar was recorded in Newtons. Method for indenting, dying and breaking was modeled closely after ASTM Standard C1421-99, for the Determination of Fracture Toughness of

Advanced Ceramics at Ambient Temperature. This method was selected because of its similarity to the strength testing that was already underway. In this case also, if any bars broke at or outside the four load points, the data was considered suspect and left out of the statistical analysis.

IV.(iii).d. Fractography

The fracture surface was kept intact after the strength testing and observed under a microscopic camera (Polaroid DMC 2.0) along with a microscopic scale. Transverse lighting source was used, that is light was incident at an inclined angle to the fracture surface of sample. A picture of the fracture surface was taken and then the critical flaw that resulted in fracture was identified as in figure-4. When looking at the surface, the crack depth is measured from the smooth surface of the bar to an area that was most clearly connected to the other fracture surface before fracture. The dimensions of the crack are then measured using Scion Image analyzer. Once the crack dimensions and strength are determined, fracture toughness is calculated. In the early work on indentation --induced flaws, the method of measurement was less precise, using a binocular wide field microscope fitted with an eyepiece camera.

IV.(iv). Results

The fracture toughness (plane strain critical stress intensity) obtained by fractographic methods from the low strength samples observed in four-point bend testing of samples from the three foundries tested. This data is shown in table 1A, along with the flaw shape parameter determined in each case. The date of sample manufacture by the foundry is noted, because process changes have been instituted at various times by the participating foundries. At foundry B a comparison test was run between the standard slurries and a proposed engineering changes using slurry that included fugitive polymer fibers.

The data obtained in the early work on indentation-induced flaws is also shown in table 1B. These samples were produced by two of the same foundries from which samples were taken for the fractographic approach. In fact the foundry C material was

form the same production batch for both methods. In both cased the breaking strength was determined by the four-point bend method described by Richards, et al (*Ref 3*). .

IV.(v) Discussion of Results

Standard deviation is smaller in the fractographic analysis than in the initial indentation work reported here. This can be attributed to better precision in image capturing and analysis than in earlier indentation work and to the use of the flaw shape parameter in the fractographic work. The earlier indentation work geometric factor Y was assigned a nominal value of unity that was improved upon in the subsequent fractography work with the introduction of the flaw shape parameter, Q, (*Ref 1*). Comparing relations (1) and (2), we get $Y=(1.21/Q)^{1/2}$. In the data reported here flaw shape parameter Q ranges from 0.75 to 2.05, while in the initial work the unity geometric factor corresponded to an assumed constant flaw shape parameter of Q=1.1.

As shown in table 1A, the mean toughness of fiber-containing samples (after the fibers were burned out) appears to be higher. To test whether the mean toughness was equal to that of shells from the same foundry without fiber, a student's t-test was performed. This gave a 5% probability that the mean fracture toughness is equal or a 95% probability that the fiber containing samples have higher toughness. This can be explained by the theory of crack deflection. When the shells with the polymer fiber are de-waxed in an autoclave, the high temperature in the autoclave causes the polymers to melt and thus leaves voids in the shell. These voids act as crack deflectors. When a crack tries to run through the shell, it hits the void and spreads to a different direction, thus giving higher fracture toughness values. The student's t-test assuming unequal variances was used for comparing the fracture toughness of similar foundries for the indented samples and the regular mold samples. The probability that the Foundry C values for different methods are equal is 23%. The probability that the Foundry B values with out fibers are equal is 27%. We can see that there is a significant but small probability that the values generated by the two methods for each foundry are equal. Based on such limited data, they may be in qualitative agreement. The indentation method needs to be refined by utilizing the improved flaw measurement methods developed in the fractography study.

The mean of fracture strength and toughness is compared in table 3. Strength is directly related with the fracture toughness: the higher the strength, the higher the fracture toughness.

The polymer fiber containing shells have greater toughness. This may contribute to their improved autoclave performance with respect to shell cracking. The observed improvements in the autoclave de-waxing of shell containing the polymer fibers had previously been totally accredited to improved permeability *(Ref 5)*.

The improvement of toughness of fired shell with the addition of the polymer fiber is probably due to crack deflection. Crack deflection can take place when there are local areas in a ceramic that have a lower resistance to crack propagation than an average plane cutting through right angles to the tensile stress *(Ref 6)*. Crack deflection mechanism is based on the tilting and twisting out of crack planes around the grains. The stresses acting in inclined planes near a crack tip depends on the angles involved. For straight cracks that, tilt is about a direction perpendicular to the crack advance through an angle θ. The stress intensity factor required for crack propagation is given by

$$K(\theta) = K(\theta=0) \sec^2 (\theta/2) \qquad (3)$$

Where: K(θ=0) is the plain strain stress intensity .

Crack propagation is diverted by a layer of porous structure due to the addition of polymer fiber material; the effective stress intensity is lessened. K(θ=0) corresponds to the apparent stress intensity measured by this technique. Thus, for the load orientation expected in de-waxing, the shell material will behave as though the fracture toughness is higher. This improvement in the toughness should also be evident in unfired shells once the fibers are melted or volatilized. However the toughness measurements in the unfired shells will be more difficult.

IV.(vi) Conclusions

The conclusions we have reached after this study are:

1. The introduction of polymer fibers in the shell, gives the shell a tougher microstructure.
2. The tougher microstructure thus produced will enhance autoclave performance relative to shell cracking.

3. The mean strengths of the shells seem to follow fracture toughness.

IV.(vii) References:

1. *George E. Dieter, Mechanical Metallurgy, Published By McGraw Hill, Third Edition, Pages 354-356.*
2. *G.R Irvin, Analysis of Stresses and Strains Near the End of a Crack Traversing a Plate, J.Appli.Mech, Vol24, pg.109-114, 1957*
3. *Von L. Richards and Ginger Connin, Four-Point Bend Testing to Characterize the Strength of Ceramic Mold Shells, Investment Casting Institute, 49th Annual Technical Meeting 2001, pg.13.1-13.10.*
4. *Francis I. Baratta, Requirements for Flexure Testing of Brittle Materials, AMMRC TR 82-20, Army Materials and Mechanics Research Center, Watertown, MA, 1982.*
5. *Dan Duffey, The Wexcoat Binder System, Investment Casting Institute, 49th Annual Technical Meeting 2001, pg.10.1-10.10.*
6. *John B. Wachtman, Mechanical Properties of Ceramics, Wiley-Interscience Publications 1996,pg. 159-163.*

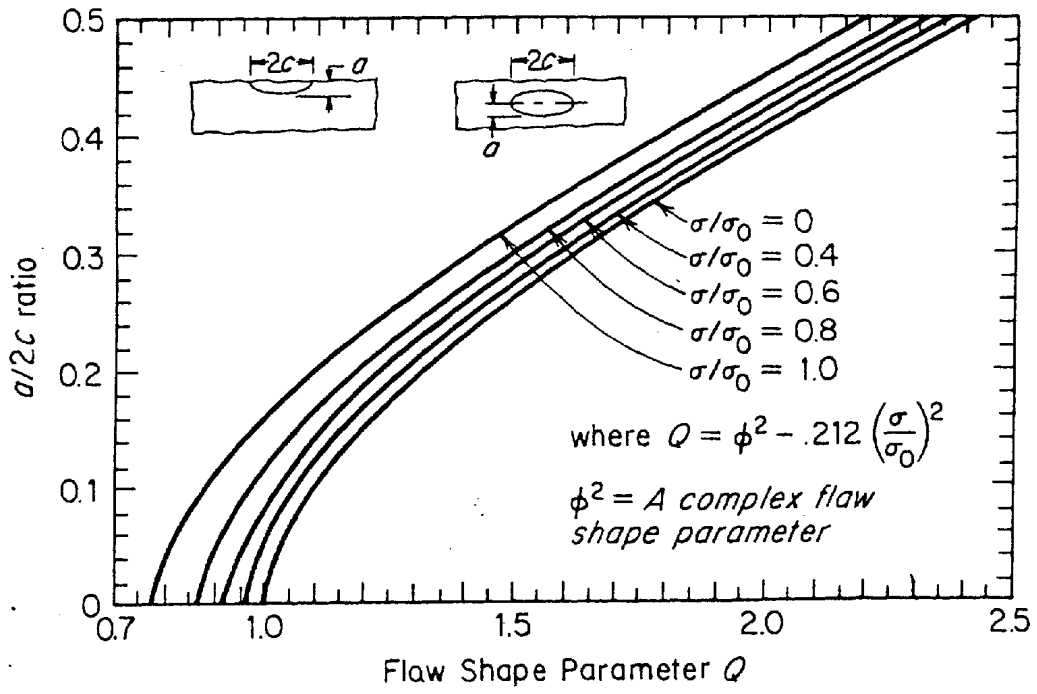

Figure-1. Flaw-Shape Parameter Q for Surface and Internal Elliptical Cracks (Ref 1)

Figure-2. Tensile Side of the Molded Test Bar

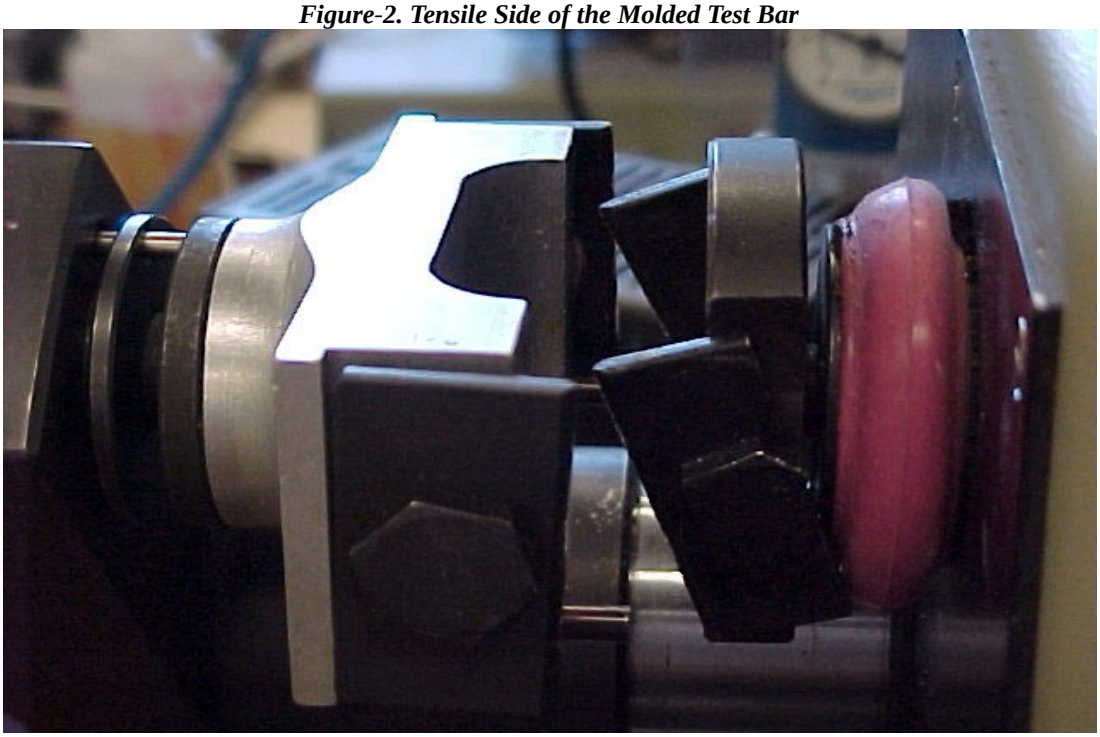

Figure-3. Four-Point Bend Apparatus.

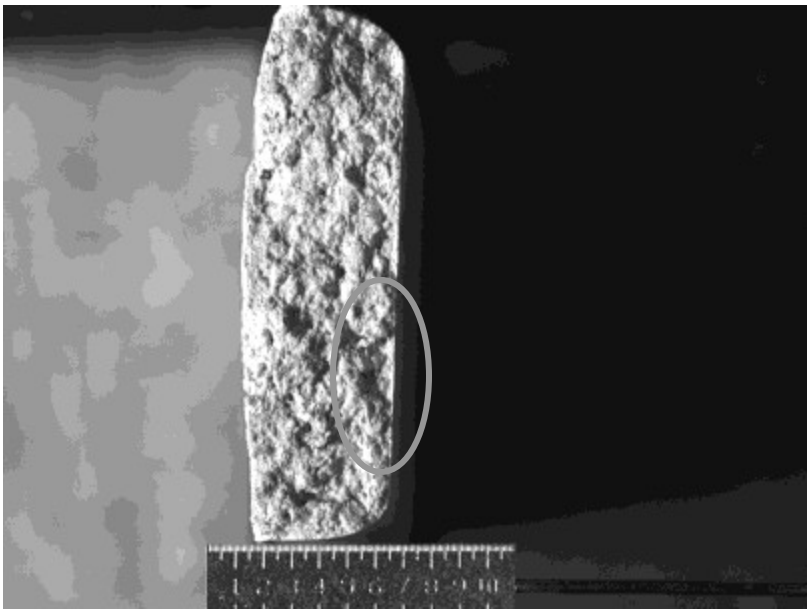

Figure-4. Fractography of Broken Bar, Oval Indicating the Critical Flaw

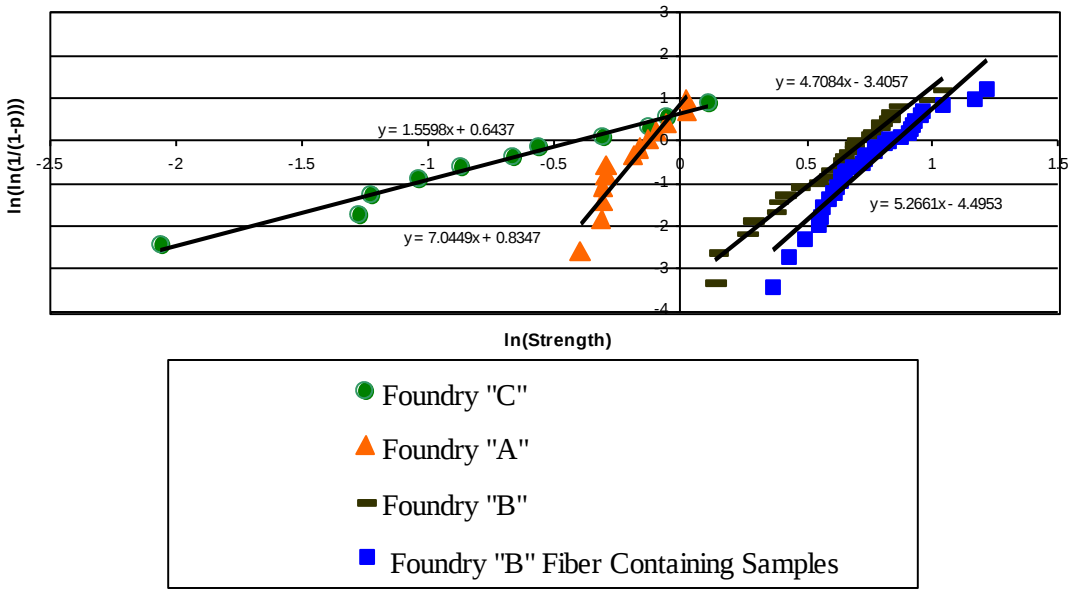

Figure–5. Comparison of Weibull Plots of Participating Foundries

Table-1A. Plane Strain Critical Stress Intensity as Determined by Fractography

Foundry-Received Date	Depth of Crack(a)		Width of Crack 2c	a/2c	Flaw Shape Parameter	Breaking Strength	Fracture Toughness (Kic)	Average Kic	Standard Deviation
	Millimeter	Meter	Millimeter		Q	MPa	Mpa(m)^0.5	Mpa(m)^0.5	
Participant A Samples Fired Without Fugitive Fibers									
	1.25	0.00125	9.43	0.132556	0.75	0.883	0.070266		
A	0.9265	0.00093	4.83	0.191822	1.1	0.736	0.041635		
6/5/01	0.4186	0.00042	1.79	0.233855	1.18	1.023	0.037557	0.050608	0.0146384
	1.566	0.00157	6.87	0.227948	1.18	0.746	0.052973		
Participant C Samples Fired Without Fugitive Fibers									
	1.35	0.00135	5.18	0.260618	1.3	0.566	0.035552		
C	1.43	0.00143	3.69	0.387534	1.75	1.118	0.062294	0.039233	0.0158326
2/9/01	1.9	0.0019	4.74	0.400844	1.8	0.515	0.032614		
	1.49	0.00149	4.59	0.324619	1.425	0.42	0.026472		
Participant B Samples Fired Without Fugitive Fibers.									
	1.9671	0.00197	3.9	0.504385	2.25	1.1435	0.065953		
	1.344	0.00134	3.0281	0.443843	1.9	2.819	0.145924		
B	1.0188	0.00272	3.3727	0.302073	1.35	1.6063	0.140541		
04/17/02	0.8913	0.00089	2.3756	0.375189	1.7	1.7928	0.079958	0.103483	0.015901
	1.4219	0.00142	3.6344	0.391234	1.75	1.1559	0.06418		
	1.895	0.0019	3.915	0.484036	2.05	2.6617	0.157949		
	1.1756	0.00118	3.4855	0.337283	1.55	1.2993	0.069878		
Participant B-Fired Samples Containing Fugitive Polymer Fibers.									
	1.46	0.00146	5.3	0.275472	1.35	3.219	0.206342		
	1.44	0.00144	4.25	0.338824	1.55	2.063	0.122567		
B	1.51	0.00151	3.29	0.458967	2	1.442	0.077232		
2/19/02	1.6	0.0016	4.57	0.350109	1.65	1.974	0.119818	0.151627	0.047311
	2.2807	0.00228	5.023	0.454051	1.95	2.286626	0.15243		
	1.0813	0.00108	3.8031	0.284321	1.35	3.045326	0.167995		
	2.1881	0.00219	6.079	0.359944	1.65	2.036294	0.144541		

Table-1B. Fracture Toughness by Indentation Method (Fired and Without Fugitive Fibers)

Foundry	Depth of Crack(a)		Width of Crack 2c	a/2c	Flaw Shape Parameter	Breaking Strength	Fracture Toughness (Kic)	Average Kic	Standard Deviation
	0.9823	0.000982	3.1293	0.31	1.41	2.4857	0.127885		
B	0.9333	0.000933	3.1293	0.30	1.4	1.1406	0.057403	0.080061	0.033666
3/15/01	0.707	0.000707	3.1007	0.23	1.18	1.568	0.074812		
	0.8389	0.000839	3.4465	0.24	1.2	1.8929	0.097555		
C	0.9006	0.000901	2.2373	0.40	1.85	2.2306	0.095931		
2/9/01	0.6102	0.00061	2.6788	0.23	1.18	1.2418	0.055043	0.058065	0.03645
	0.4262	0.000426	1.8361	0.23	1.18	0.6268	0.023219		

Table- 2. Toughness Comparison of Samples with Fugitive Fibers and Samples without Fugitive Fibers from Foundry B

	Fibrous Sample 2/19/02	Non -Fibrous Sample-- 4/17/02
Average Toughness	0.151627	0.103483348
Standard Deviation	0.047311151	0.015900956
Sample Size N	8	7

Table-3. Toughness and Strength Comparison of Participating Foundries

Foundry	Mean Strength	Mean K_{1c}
A	0.834	0.0506
B	1.889	0.1034
C	0.5674	0.039233
B Containing Fugitive Fibers	2.165	0.1516

V. THERMAL EXPANSION OF INVESTMENT CASTING PATTERN WAX.

By

Student Participants; Sony Mascreen, Brian Sutherland, Phil Jackson, Adrienne Orf

And

Dr.Von L. Richards, Ph.D.

University of Missouri at Rolla

V.(i) Introduction:

The purpose for testing the thermal expansion of pattern wax is due to the effect of the free strain developed during autoclave de-waxing. Typically investment-casting shell cracking may occur at combinations of high load and high stress intensity. The wax expansion during mold de-waxing imposes stress on shell since thermal expansion of shell is lower than that of wax. The expanding wax induces stress onto the inner surface of shell, which sometimes is the cause of shell cracking. It is a widely held paradigm that autoclaving causes shell cracking. Although knowledgeable ceramic engineers working in the investment casting industry will admit that the flaw population introduced in shell production affects the resistance to cracking, the effects often appear during autoclave de-waxing. Therefore, it is also reasonable that the mechanical properties of the pattern wax will affect performance during the de-wax cycle.

Our fixture is made of aluminum, which surrounds the wax on all the sides but one, which enables an excellent heat transfer. There is a glass slide on the side of wax that isn't covered by aluminum, which allows us to observe the change in length of wax. There is a rectangular aluminum plug also, as seen in figure 4, which keeps the flow of wax uniform when it reaches liquid state.

The thermal expansion of investment casting pattern wax has been measured by a non-contact method from room temperature up through the melting temperature. The effects of the following variables on thermal expansion have been examined: section thickness, orientation with respect to injection flow, injection pressure, heating rate, and recycling procedure. It is clear that heating rate affects the temperature at which one observes the onset of relaxation of the non-crystalline portion of the structure. A higher heating rate raises the relaxation temperature and the thermal expansion that occurs before the structural relaxation. Thinner sections can cool more rapidly and affect the degree of crystallinity and free volume of the non-crystalline portion of the wax structure. Recycling procedures tend to affect the volume change upon melting the crystalline portion of the wax structure. This is an abrupt volume increase and can apply significant stress to the shell during autoclaving. Filled and unfilled waxes from participant foundries were examined as well as virgin waxes suggested by vendors.

V.(iii) Procedure

The waxes used for these experiments are obtained from the participating foundries. These foundries inject wax into the wax step block pattern to provide samples. The wax is injected at three different injection pressures; (1) the normal injection pressure of the foundry, (2) 100 psi higher than normal and (3) 100 psi lower than normal. Vendor waxes are injected either by the vendor or by a participating foundry. Figures 1 and 2 show the wax step block pattern. The steps are 0.25 inches, 0.375 inches and 0.5 inches thick. The injection direction is parallel to the steps.

V.(iii).a. Machining The Wax

The first step in preparing a wax specimen for experimentation is to machine a small sample strip from the wax step mold. This is done by using a vertical band saw, a vertical milling machine and final sanding with 400 grit sand paper. The wax strip is

machined to give a good fit in the test cell channel. To avoid annealing the wax, it is refrigerated between each of the machining steps to insure that premature heating does not occur. Once the wax is completely machined, the test cell itself must be prepared.

V.(iii).b. Test Cell

The test cell is made of aluminum with a cover glass and a slider to follow the wax. The first step in the preparation of a test cell is simply cleaning it by using a light dishwashing soap. It is then rinsed and dried thoroughly. A small layer of vacuum grease is applied to the inner-faces of the aluminum top, bottom, and slider. The slider is lubricated with vacuum grease so that it provides a non-contact measurement method. A small amount of no-stick solution is placed inside the channel where the wax will be tested. The wax strip is inserted into the test cell channel. Once all of these preparations have been made, the cell is bolted together and put back into the refrigerator. The assembled and disassembled test cell is shown in figures 3 and 4.

V.(iii).c. Setting Up The Experimental Apparatus

In order to get a highly accurate measurement of the expanding wax, experimental apparatus is set up underneath a microscopic camera (Polaroid DMC 2.0). The test cell is partially submerged in a water bath that sits on top of a hot plate. A feedback thermocouple is positioned in the water bath. This way, the water temperature can be controlled by the hot plate. Additional thermocouples are located inside the aluminum body of the test cell. These temperatures are then read using two-port digital thermocouple readout. Figures 5 and 6 show the test cell set-up.

V.(iii).d. Procedure For Length Measurement

A series of pictures of the wax is taken at different temperatures with a microscopic camera. Scion Image analysis software is used to measure the wax lengths from the pictures. Earlier measurements in this study used a video coordinate measuring machine to measure the length at the same time increments as currently used with the Polaroid DMC in recent measurements.

V.(iii).e. Procedure For Slow Heating Process

When the slow heating process is being used, the sample is started below room temperature. A length measurement is taken, and then the test cell is allowed to equilibrate with the room temperature by adding water. Once room temperature is

reached, another length measurement is taken. From this point on, the test cell is heated at a rate of 3°C with length measurements being taken between each 3°C increment (roughly seven to nine minutes between increments to get an equilibrium temperature). The entire process lasts until the wax reaches a temperature of about 60 to 65°C. At this temperature, the wax is mostly liquid. The experiment is terminated when the liquid wax starts to leak past the slider. A typical measurement cycle requires two and one-half hours.

V.(iii).F. Procedure For Accelerated Heating Process

Similar to the slow heating process, the sample is started below room temperature. An initial length measurement is taken, and then the water is applied to the test cell and is allowed to equilibrate to room temperature. From this point, the hot plate is set at 300°C, and measurements are made at three-degree increments. The entire set of measurements takes about eight minutes.

V.(iv) Results:

As a result of performing thermal expansion tests on pattern waxes, we were able to better examine many of the thermal properties for these waxes. We used several different experimentation methods to help broaden the amount of information we could obtain for a wax. Some of the different experimental approaches included looking at mold injection pressures, injection flow rates, water quenched waxes, recycled versus virgin waxes, wax thickness, heating rates, and wax orientation. The results for each of these tests will be discussed in this section.

V.(iv).a. Wax Thickness

One of the first tests that we performed on a pattern wax was designed to determine the effect of wax thickness. To perform this test, we designed a step block mold that would be used for the duration of the program. This block consisted of three different thicknesses: .25 in, .375 in, and .5 in. All three different thicknesses were tested using the same experimental setup and procedure. Once all the data was collected, the resulting graphs were compared. From these graphs, we were able to determine that the thicker sections expand at a slightly smaller rate than the thinner sections (figures 7 and 8). Also, the majority of the expansion difference between the two wax thicknesses was

present where all of the crystalline material transformed into liquid. This can possibly be related to the pressure at which the wax was injected. This causes the amount of crystalline material in the wax to increase.

V.(iv).b. Recycled Wax vs. Virgin Wax

Another test that was performed on the waxes was developed to determine how recycled waxes compare with virgin waxes. We used the same thickness in our study to eliminate the cooling rate factor. Figure 9 showed that recycling of the cerita 29-51 had the same effect as reported by for participant "A" recycled versus virgin wax – a greater crystalline expansion portion of the curve with there recycled wax. To be more precise, it should be noted that this effect was less significant with the Cerita 29-51 and the participant "C" recycling system than was indicated in earlier work for foundry "A".

It is very important to note that different recycling procedures will yield different properties within the wax (figure 10). Recycled wax #1 and #2 were prepared using two different reclaim methods. As is evident from the graph, recycled wax #1 has a great deal of crystalline expansion present while the other recycled wax shows more expansion while the wax is still solid. Although neither recycling process was able to perform as a virgin wax, the second recycled wax was very similar in the amount of crystalline expansion.

V.(iv).c. Injection Pressures

To conduct this experiment, we used a wax injected at three different pressures from the same participant. The three pressure levels were one the normal injection pressure of the participating foundry and other two were 100 psi lower and 100 psi higher to the normal pressure. Again, they were tested using the same setup and procedure. The same thickness was again used to avoid the cooling rate factor. Figure 11 and 12 illustrates the effect of injection pressure. Assuming that we did not overlook any entrapped gas bubbles, the high injection pressure may have resolved several crystalline melting events due to blended molecular weights. Also, the main crystalline melting event is produces a more significant volume increase when higher injection pressures are used. The higher the pressure, the more crystalline melting expansion can be observed.

V.(vi).d .Vendor Waxes

As our study with waxes continued, a few participants asked that we examine some commercial waxes to help reference our data. The main thrust of the work done during this year in the wax expansion area was to examine the wax used by Sabau, et al (Sabau, 2001) at Oak Ridge National Laboratory to help provide a reference benchmark for the participating foundry waxes that have been examined in this program. Coincidentally, Participant C was using the same wax, Cerita 29-51, but they used reclaimed wax for patterns as well as sprue and had a very thoroughly controlled staged reclamation system. This provided an opportunity to compare reclaimed Cerita 29-51 to as-received or "virgin" wax. The vendor and participant C injected these waxes. The effects of pattern section thickness and injection pressure were also examined.

The participant foundries recommended examining some commercial waxes to provide a reference for the database. Remet, and Kindt Collins offered their best "starter wax". "Starter wax" is defined as their recommendation to a caster starting an investment casting process. Cerita 29-51 was used to reference the Oak Ridge study, (Sabau et al 2000). Figure 13shows comparison of all the vendor and participant waxes to date. This gives participating foundries a means to relate their wax to the vendor waxes and other research.

V.(iv).e. Injection Flow Rate

The thermal expansion of wax injected at different flow rates were tested. The wax we used for this was from participant D. The different flow rates used by the participants were

1. Low flow rate (Flow rate of 2 on a scale of 1- 10)
2. Control flow rate (Flow rate of 3 on a scale of 1- 10)
3. High flow rate (Flow rate of 7 on a scale of 1-10)

We also compared the thermal expansion of these waxes with the water-quenched wax injected at a control flow rate. These waxes are water quenched in 109 degree F water for 1 hour).

Figure 14 shows the comparison of different injection rates of participant D wax. The low flow rate wax showed more crystalline expansion when compared to the control flow rate and water quenched wax injected at the control flow rate.

Water quenching the wax injected at the control flow rate didn't show any difference in the linear thermal expansion of the wax when compared with the wax injected at the control flow rate. Higher injection shear rate of wax doesn't seem to increase the formation of crystalline components in the wax. The formation of the crystalline material is dependent upon the injection pressure only. We were unsuccessful in getting repeated thermal expansion results from the high flow rate waxes. This was due to the numerous air bubbles in the wax step block and this in turn gave erroneous results.

V.(iv).f. Wax Orientation

We did complete one study that involved testing waxes that were parallel and perpendicular to the wax injection direction. They were the same thickness and were tested using the same procedure. There was very little difference between the two as far as expansion was concerned. The results for this test can be seen in figure 17.

V.(iv).g. Heating Rates

Another experiment that was used to test the pattern wax involved changing the rate at which it was heated. For our testing, we have used two different heating rates. The first rate is a very slow heating process that takes the wax from roughly 15°C to 70°C in about 2.5 hours. With this process, we can clearly see any critical temperatures such as the glass transition temperature. We can also observe when the crystalline material transforms into a liquid substance. It was important to apply this type of heating rate so that we would be able to get a very close idea of the characteristics of the wax. The second heating process took the wax from 15°C to 70°C in nearly 8 minutes. We used this rapid heating rate to try to replicate an actual autoclave process. Again, we are able to see critical temperatures and phases, but this time we are observing how the wax would act in an actual manufacturing environment. Once we had collected an adequate

amount of data for each heating rate, we made a comparison between the two (figure18). As one can see, the amount of crystalline material that goes into liquid is very similar between the two heating rates, but the temperature at which the amount of volume relaxation occurs is different. The onset of volume relaxation occurs at a higher temperature with faster heating.

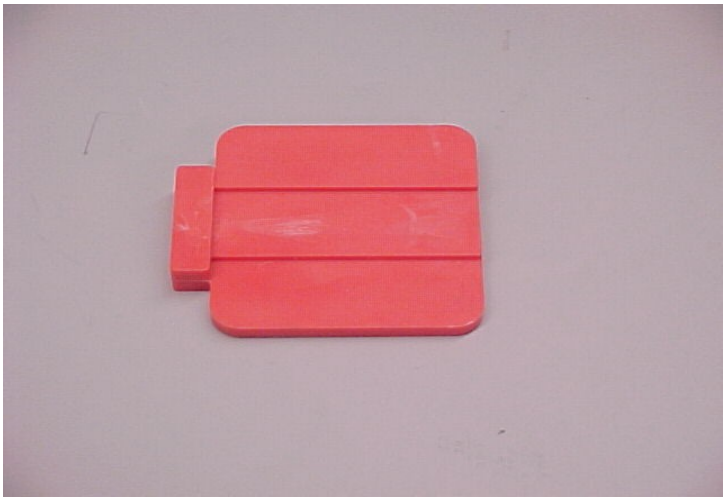

Figure 1: Top view of wax step block

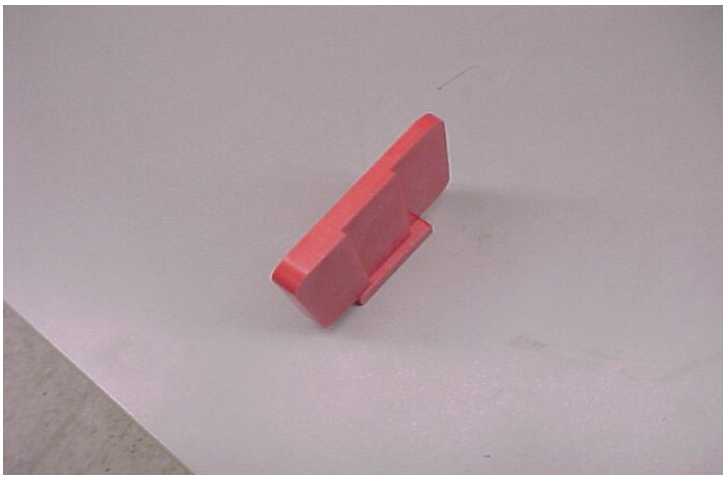

Figure 2: Side view of wax step block

Figure 3: Top view of disassembled test cell

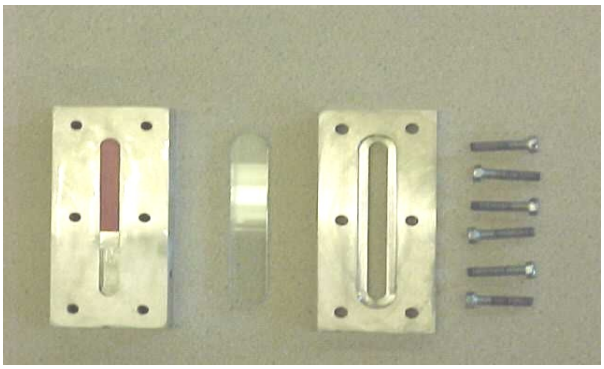

Figure 4: Top view of the assembled test cell

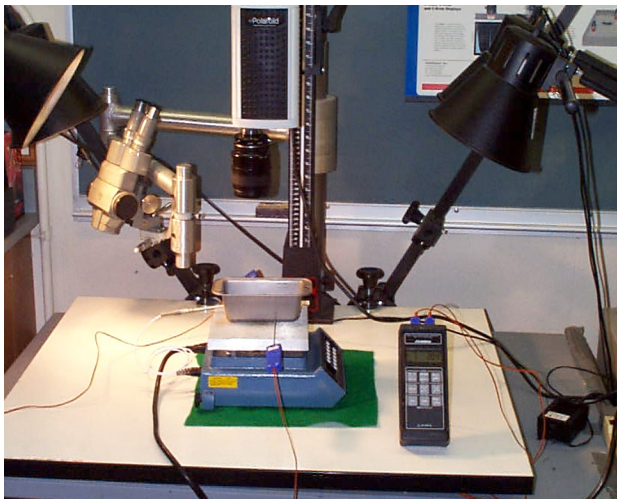

Figure 5: Complete Experimental Apparatus

Figure 6: Water Bath and Hot Plate Setup

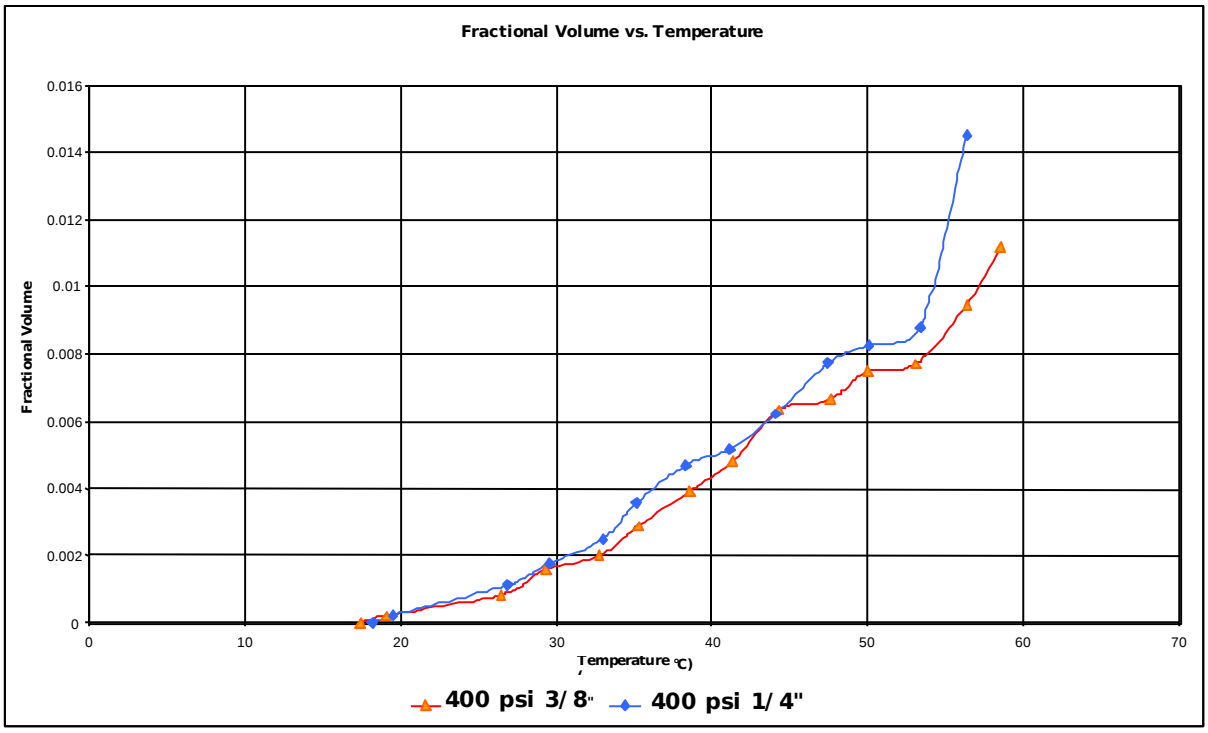

Figure7: Comparison of Participant C Wax of Different Thickness

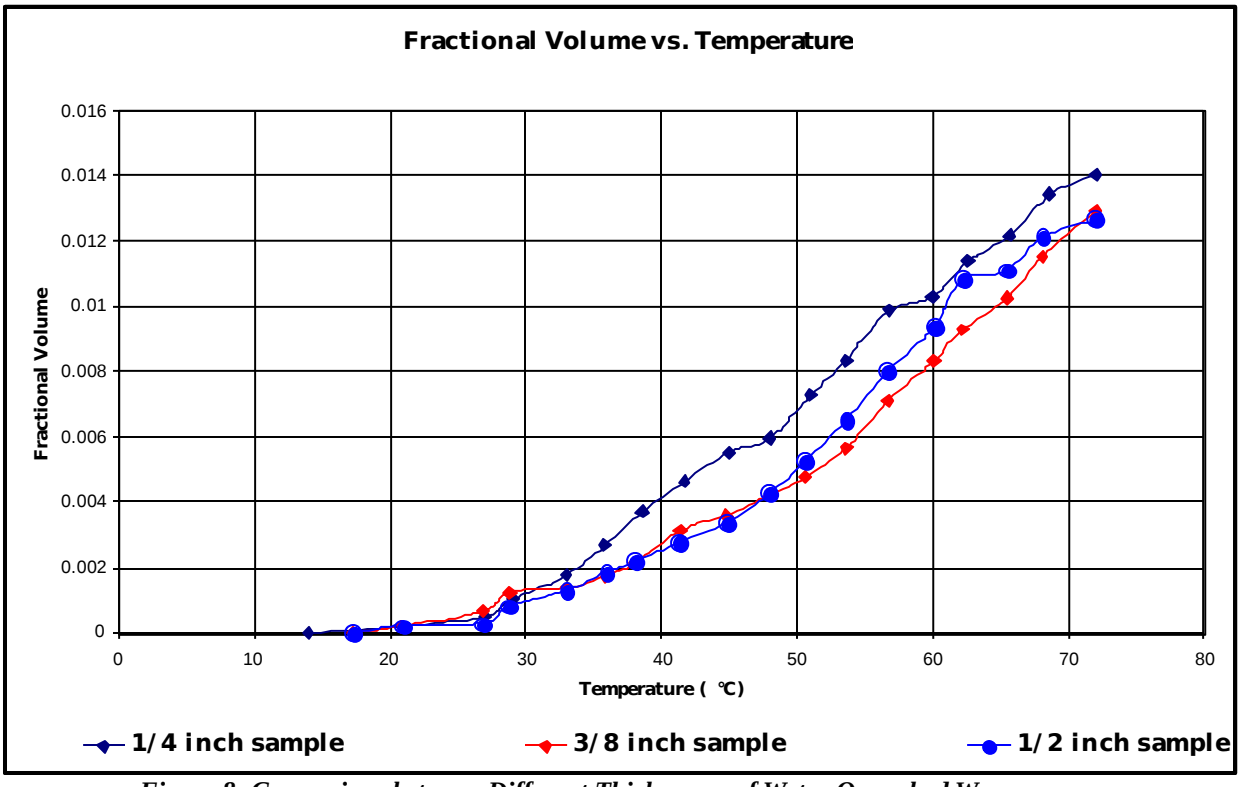

Figure 8: Comparison between Different Thicknesses of Water-Quenched Wax

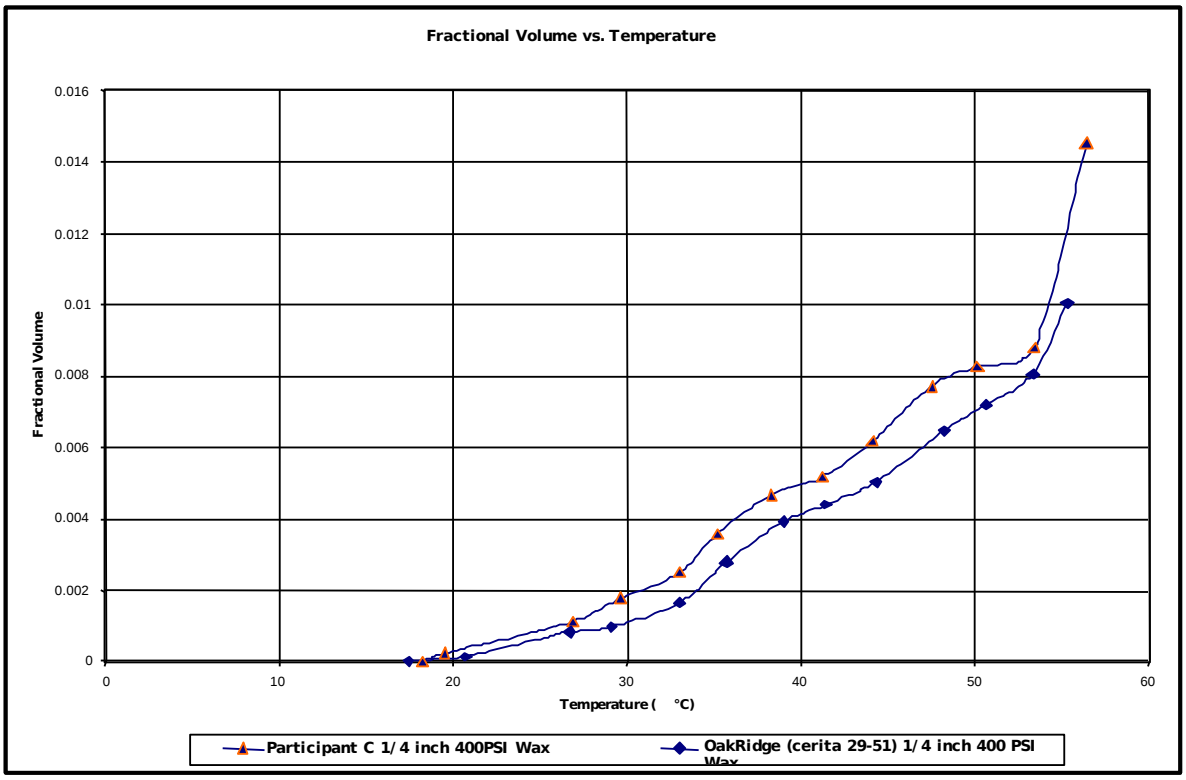

Figure 9: Comparison of Cerita 29-51 Virgin Wax to Recycled Wax (Cerita 29-51 from participant C)

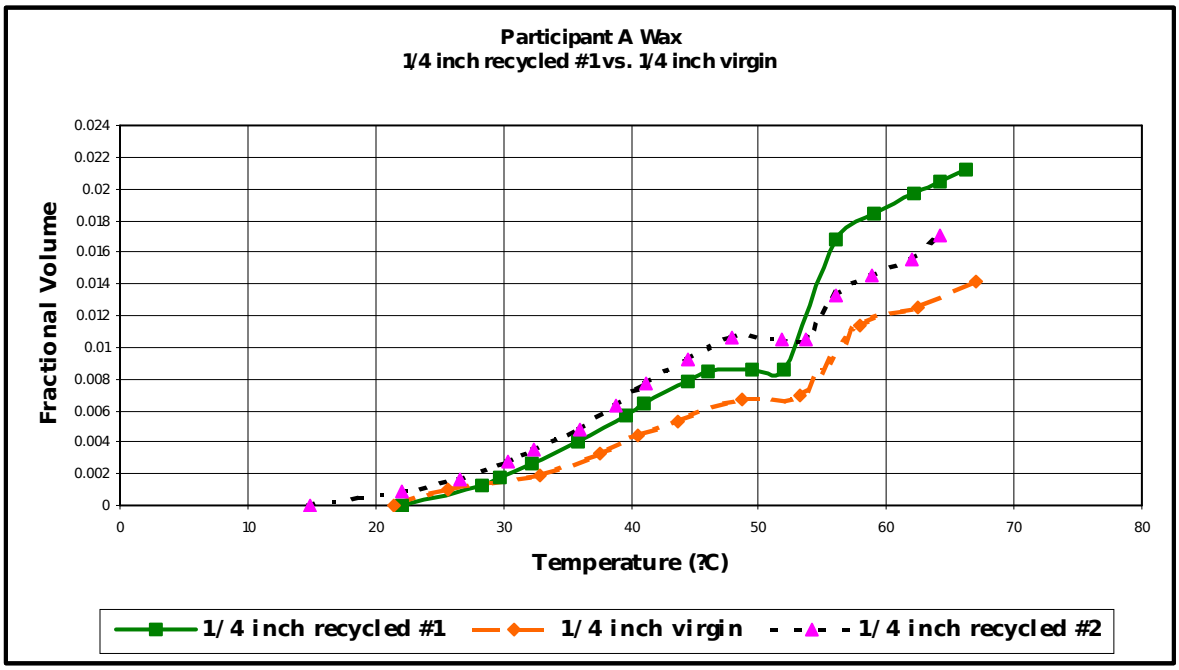

Figure 10: Comparison Recycling Procedures of Participant A Wax with Virgin Wax

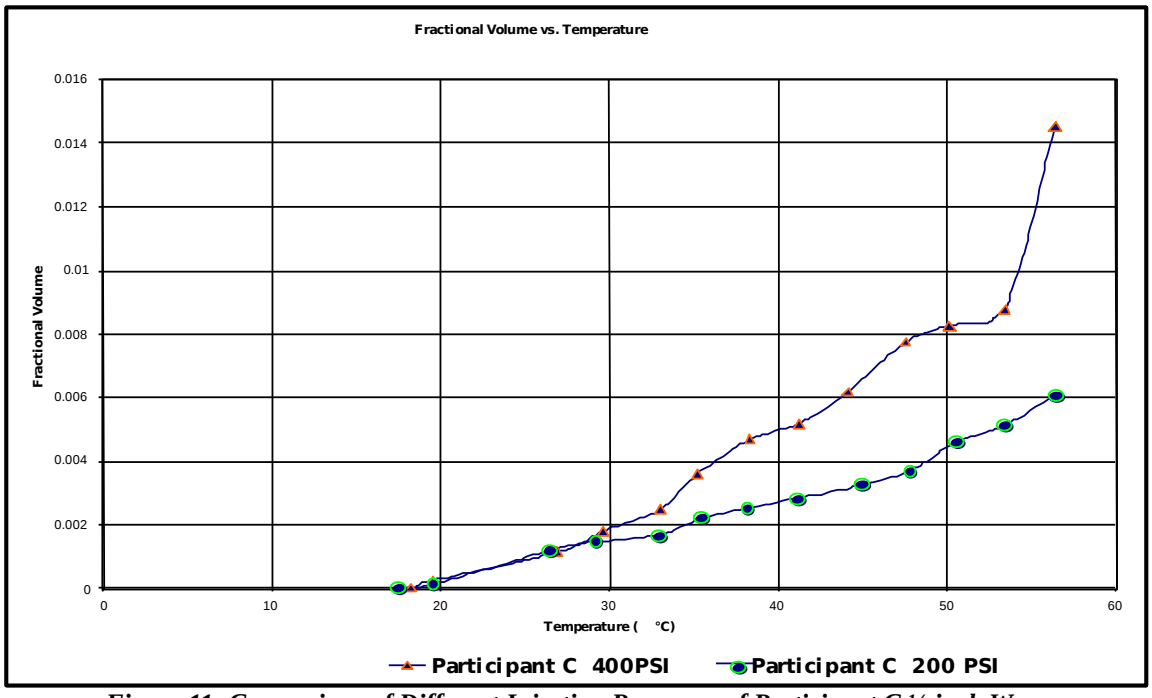

Figure 11: Comparison of Different Injection Pressures of Participant C ¼ inch Wax

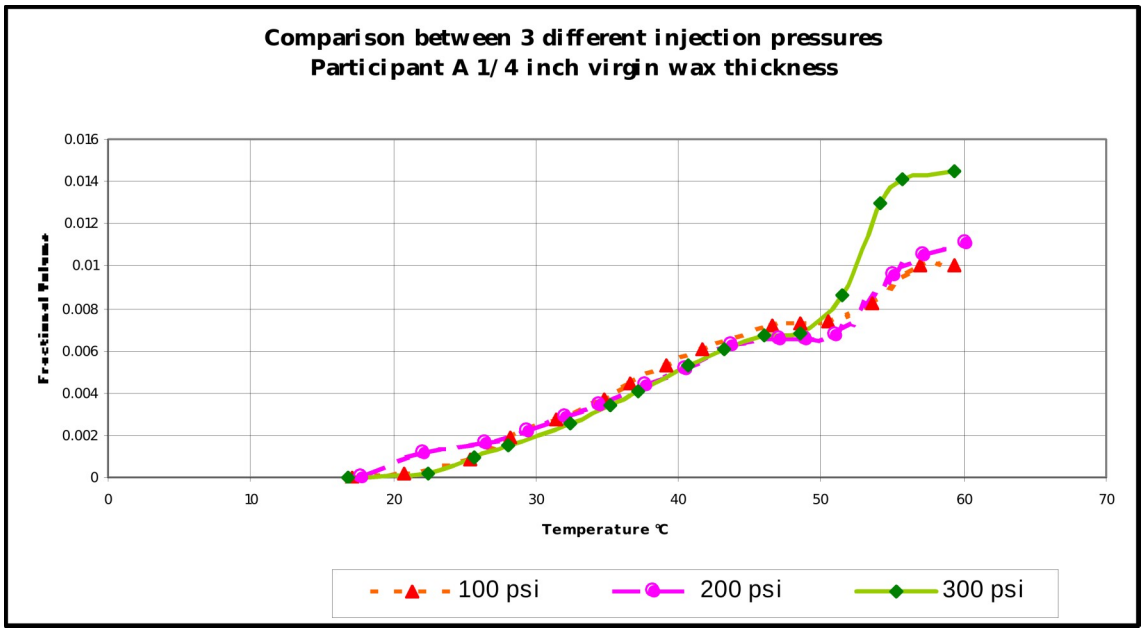

Figure12: Comparison of Different Injection Pressures of Participant A Wax

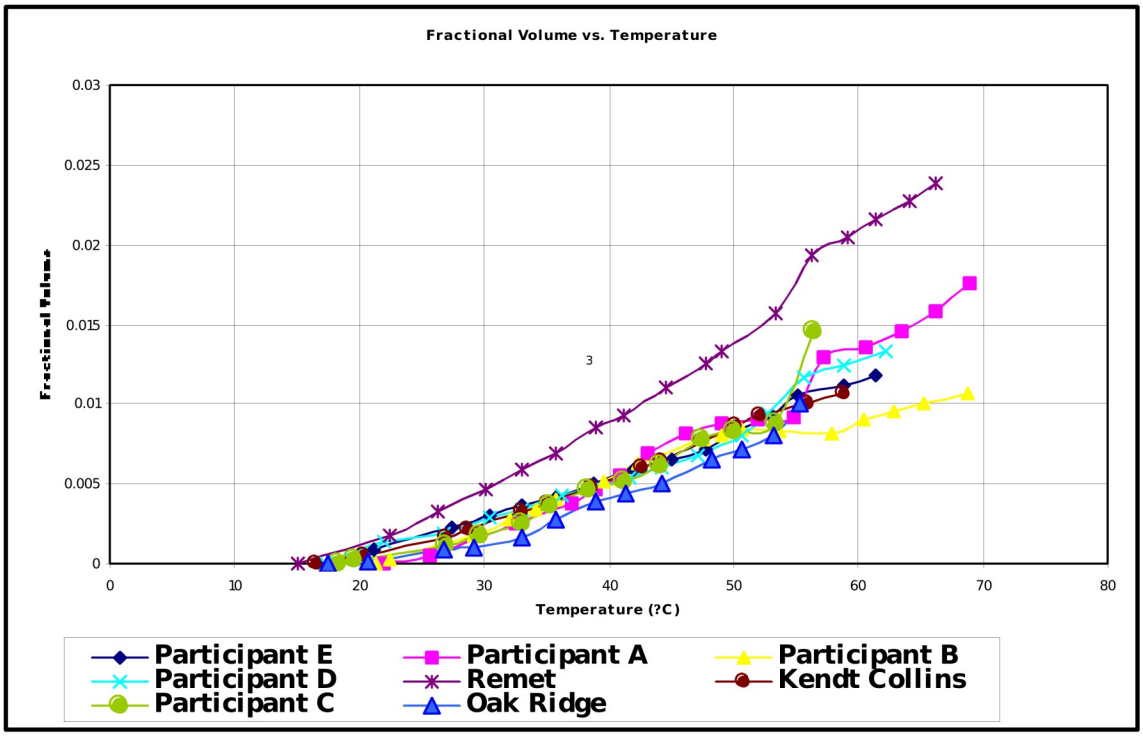

Figure 13: Comparison of Different Vendor Waxes to Participant Waxes

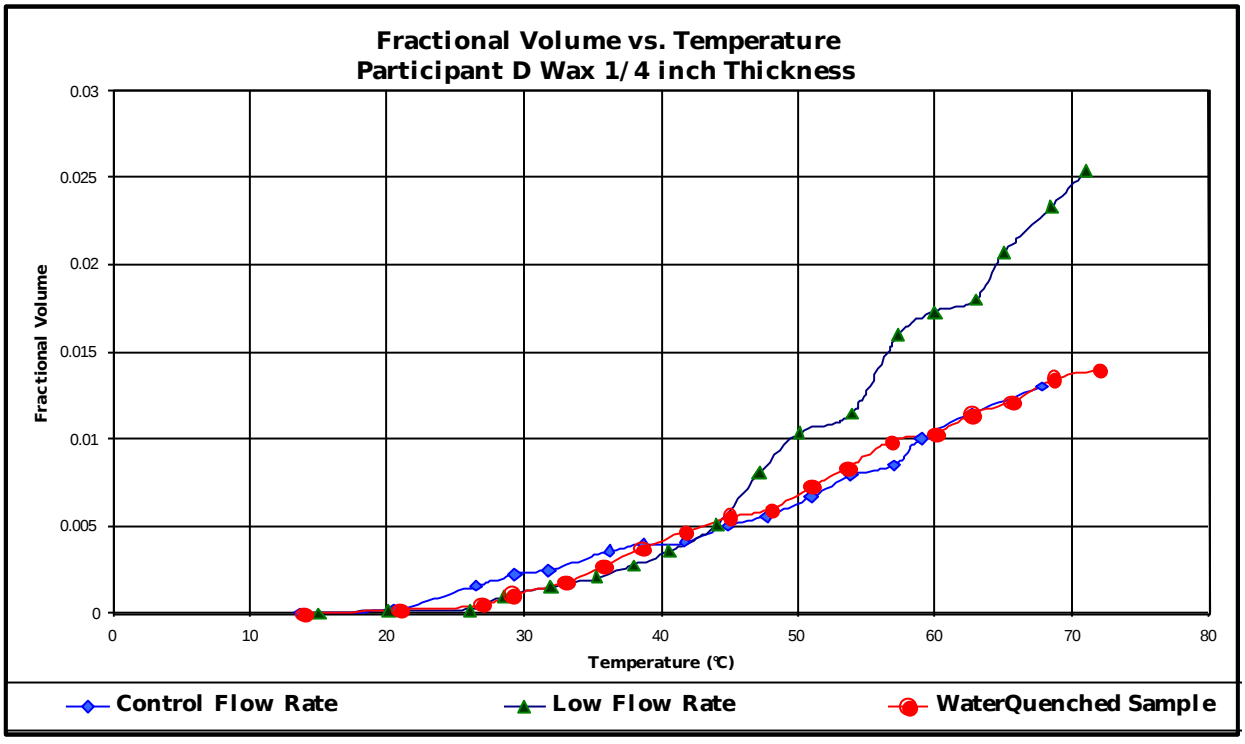

Figure14: Comparison of Different Injection Flow Rates

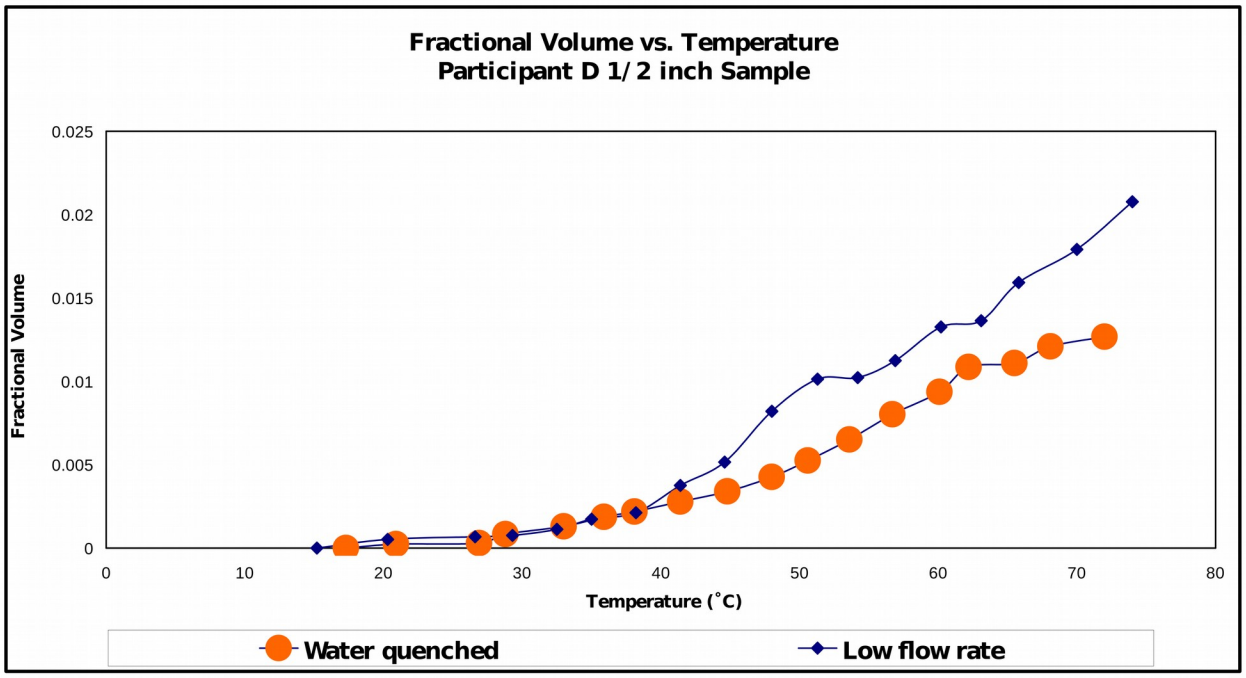

Figure 15: Comparison of Water Quenched Wax with Low Flow Rate Wax

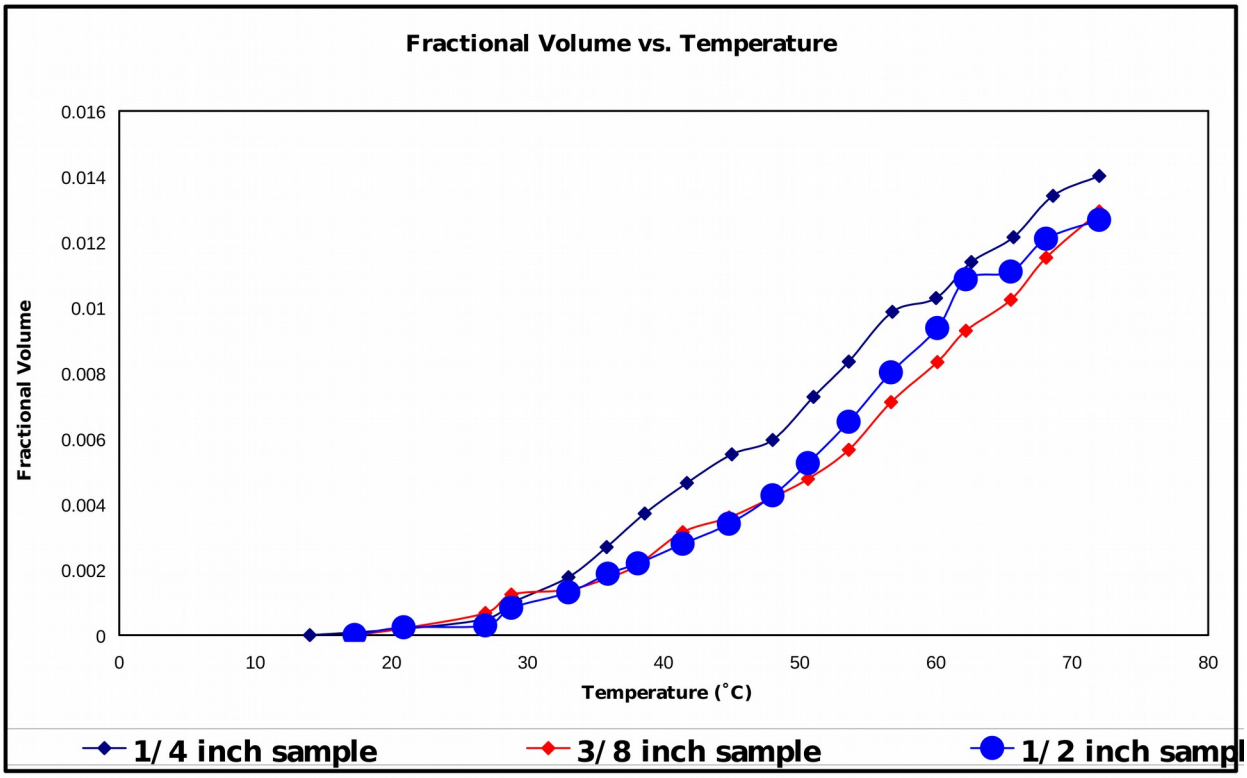

Figure 16: Comparison between Different Thicknesses of Water-Quenched Wax

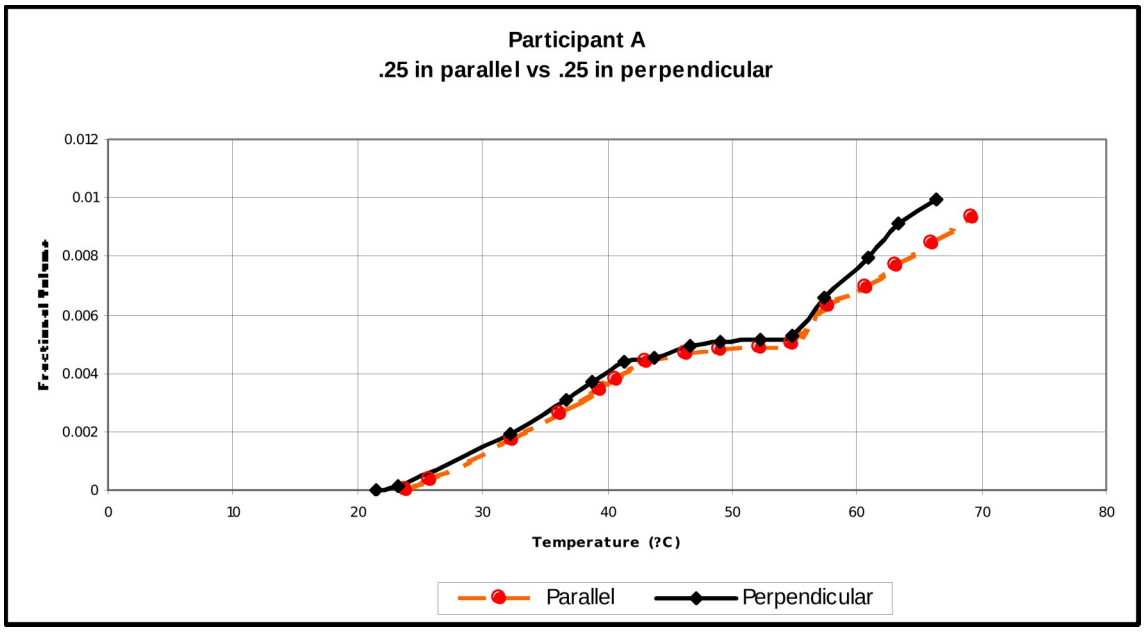

Figure17 Comparison of Thermal Expansion of Wax with Different Orientation

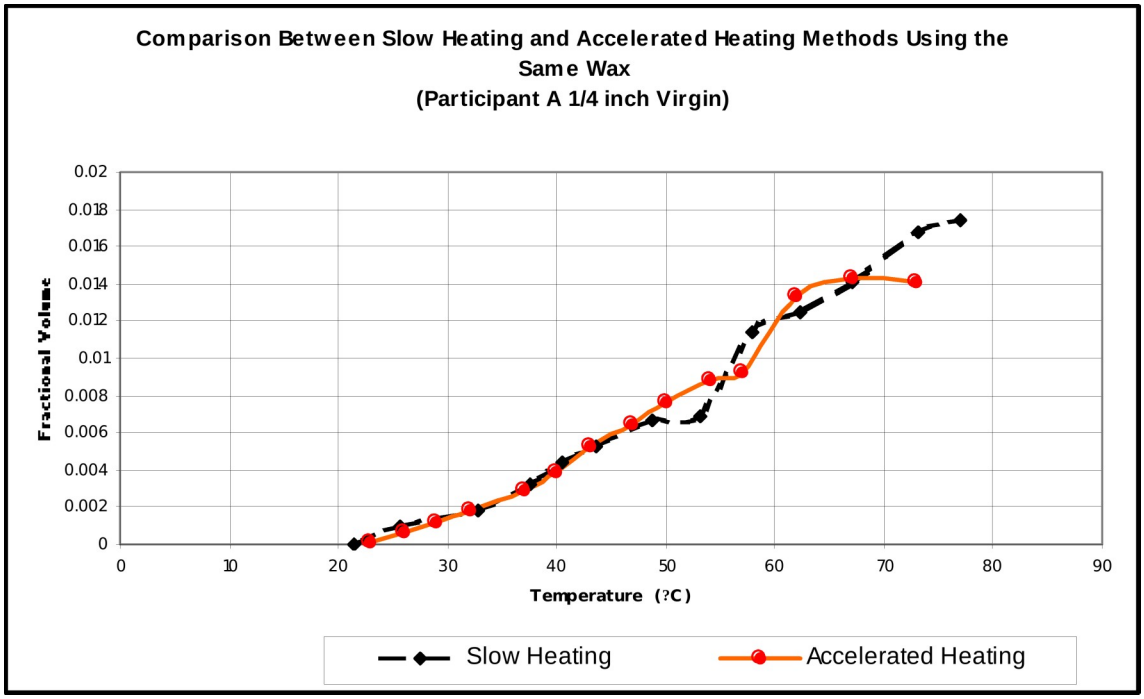

Figure18 Comparison of Thermal Expansion of Wax with Different Heating Rates

VI. Sonic Test For The Determination Of Young's Modulus

By

Teck-Sang "Chris" Tan (Student Participant)

And

Dr. Von L. Richards.

VI.(i) Introduction:

Sonic testing is a nondestructive testing used to determine the elastic modulus or Young's modulus. The reason for using this test is to obtain a guideline for four-point bend test that determines the stress of the ceramic shells of participating members. During the coordination meeting in January 2001, a question was raised about the apparent inverse correlation between strength and elastic modulus in the early data. We have explored this relationship on two batches of ceramic bars from two foundries, with concurrent strength testing on the same bars. These bars are thinner than the normal test bar we have been using, which leads to a little more scatter in the strength result. These foundries will be named as foundry M and foundry H. Research was carried out to choose the best way doing the test and after referring to some sources, a test using speed of sound was carried out. Referring to ASTM C1259-98 (Standard Test Method for

Dynamic Young's Modulus, Shear Young's Modulus, and Poisson's Ratio for Advanced Ceramics by Impulse Excitation of Vibration).

VI.(ii) Results:

Referring to Table III-1 (Foundry M), Table III-3 (Foundry M) and Figure III-1, there is a noticeable relationship of the elastic modulus to the strength of the bars. By taking the result obtained from the four-point bend test, the strength of two test bars (1_1 and 2_4) is almost the same (at about 10.92 MPa), but there is a big difference in their elastic modulus values from the sonic test (about 4 GPa). Then, referring to the result obtained from bar 3_3, this bar has the highest strength (16MPa), but it has about the median elastic modulus value. When we examine the test results obtained from foundry H (Please refer to Table III-2, Table III-5 and Figure III-2), the elastic modulus and the strength of the test bars have narrow distributions (mean for the elastic modulus is 7.20 GPa and the standard deviation is 1.4 GPa; mean for the strength is 3.1MPa and standard deviation is 0.45MPa). Why is there such a great difference between these two batches of bars from these two foundries? Pore size distributions were found to be substantially different. The bars from Foundry M have a broader distribution of pore sizes. One might suggest that the pore size controls strength, while the pore volume fraction controls the elastic modulus of the bars. For example, as shown in Figure III-3a, Figure III-3b and Figure III-3c, it is found that the structure of the bar that has a more regular structure gave the highest value compared to the other two bars. However, the bars from Foundry H have a more regular and dense microstructure compared to Foundry M.

The result, which was plotted as strength versus the Young's Modulus has a specific relationship for the bars, tested for Foundry M, as shown in Figure 2. Mathematically speaking, the curve was a second power polynomial curve. The student participant was asked to explain the phenomenon, and he found that the relationship is due to the pore volume and size distribution in the ceramic bars. This may follow the relationship derived by J.K. MacKenzie, $E=E_0(1-1.9P+0.9P^2)$ (P-pore volume fraction, E_0-matrix elastic modulus, and E- elastic modulus of sample) to describe the change of elastic modulus due to the addition of low modulus material as second phase. Specifically, we add pore spaces that have approximately zero bulk modulus values

(Kingery, p.775.) If the strength is proportionate to non-pore volume, while modulus involves a second power term, a second power relationship of strength to modulus is reasonable.

The modulus results suggest predicting the strength of the bars that are from the same foundry before testing them with the four-point bend test. But, this does not conclude that the modulus test is a reliable predictor of strength.

Table 1 -- Foundry M Results from Sonic Modulus Test

Calculation for Young's Modulus for test bar
Date: 2/26/01
Foundry name: M
Received: 02-09-01

b(mm)	L(mm)	t(mm)	f (Hz)	T_1	m (g)	E (GPa)	L/t	density	Type
21.42	130.16	6.17	1888	1.015	132	198.6778	21.1	7.6967	a-36
25.593	100.73	5.03	4960	1.016	49.9	369.8704	20.01	3.8456	alumina
20.18	130.32	6.39	1856	1.016	45.2	62.92835	20.39	2.6897	aluminum
19	98.01	4.5	896	1.014	12.5	5.236655	21.78	1.4917	1_1
19	98.01	4.5	864	1.014	12.5	4.869287	21.78	1.4917	1_1
19	98.01	4.5	896	1.014	12.5	5.236655	21.78	1.4917	1_1
19.13	98.85	4	800	1.011	11.2	5.410177	24.71	1.4807	1_3
19.13	98.85	4	800	1.011	11.2	5.410177	24.71	1.4807	1_3
19.13	98.85	4	800	1.011	11.2	5.410177	24.71	1.4807	1_3
19.1	98.4	4.8	768	1.016	13.2	3.375962	20.5	1.4632	3_5
19.1	98.4	4.8	896	1.016	13.2	4.595059	20.5	1.4632	3_5
19.1	98.4	4.8	768	1.016	13.2	3.375962	20.5	1.4632	3_5
19.1	98.05	4.85	704	1.016	13.2	2.721859	20.22	1.4533	3_2
19.1	98.05	4.85	768	1.016	13.2	3.239237	20.22	1.4533	3_2
19.1	98.05	4.85	736	1.016	13.2	2.974924	20.22	1.4533	3_2
19.18	97.8	4.89	672	1.016	13	2.355783	20	1.4173	3_1
19.18	97.8	4.89	672	1.016	13	2.355783	20	1.4173	3_1
19.18	97.8	4.89	640	1.016	13	2.136765	20	1.4173	3_1

19.12	98.38	4.6	928	1.014	12.3	5.203416	21.39	1.4215	2_3
19.12	98.38	4.6	896	1.014	12.3	4.850746	21.39	1.4215	2_3
19.12	98.38	4.6	928	1.014	12.3	5.203416	21.39	1.4215	2_3
19.1	98.47	4.85	768	1.016	14.1	3.504276	20.3	1.5458	3_3
19.1	98.47	4.85	640	1.016	14.1	2.433525	20.3	1.5458	3_3
19.1	98.47	4.85	896	1.016	14.1	4.769709	20.3	1.5458	3_3
19	98.92	4.23	864	1.012	11.5	5.535052	23.39	1.4465	2_2
19	98.92	4.23	736	1.012	11.5	4.01652	23.39	1.4465	2_2
19	98.92	4.23	832	1.012	11.5	5.132641	23.39	1.4465	2_2
19.07	98.55	4.8	608	1.016	12.9	2.080391	20.53	1.43	2_4
19.07	98.55	4.8	576	1.016	12.9	1.867165	20.53	1.43	2_4
19.07	98.55	4.8	576	1.016	12.9	1.867165	20.53	1.43	2_4
21.42	130.16	6.17	1888	1.015	132	198.6778	21.1	7.6967	a-36
25.593	100.73	5.03	4960	1.016	49.9	369.8704	20.01	3.8456	alumina
20.18	130.32	6.39	1856	1.016	45.2	62.92835	20.39	2.6897	aluminum

Table 2 -- Foundry H Results for Sonically Determined Modulus

Foundry:H
RECEIVED: 3-15-01
TEST DATE:03/30/01

b(mm)	L(mm)	t(mm)	f (Hz)	T_1	m (g)	E (GPa)	L/t	density	Type
21.5	130.2	6.13	1888	1.01	133	202.42	21.2	7.742	a-36
25.6	100.6	5.03	4864	1.02	49.9	354.41	20	3.859	alumina
20.1	130.3	6.35	1856	1.02	45.4	64.586	20.5	2.725	aluminum
18.9	94.2	3.74	864	1.01	12.7	7.665	25.2	1.907	H1
18.9	94.2	3.74	832	1.01	12.7	7.1077	25.2	1.907	H1
18.9	94.2	3.74	800	1.01	12.7	6.5715	25.2	1.907	H1
19.1	100.5	4.1	864	1.01	15	8.2837	24.5	1.911	H5
19.1	100.5	4.1	992	1.01	15	10.92	24.5	1.911	H5
19.1	100.5	4.1	800	1.01	15	7.1019	24.5	1.911	H5
19	89.13	3.6	992	1.01	11.5	8.6475	24.8	1.886	H6
19	89.13	3.6	704	1.01	11.5	4.3553	24.8	1.886	H6
19	89.13	3.6	832	1.01	11.5	6.083	24.8	1.886	H6
18.9	97.59	4.5	928	1.01	16	7.1253	21.7	1.925	H9
18.9	97.59	4.5	928	1.01	16	7.1253	21.7	1.925	H9
18.9	97.59	4.5	992	1.01	16	8.142	21.7	1.925	H9
18.9	95.74	3.9	960	1.01	14.5	10.035	24.5	2.06	H13
18.9	95.74	3.9	832	1.01	14.5	7.5375	24.5	2.06	H13
18.9	95.74	3.9	896	1.01	14.5	8.7418	24.5	2.06	H13
19.1	100.2	4.5	960	1.01	15.2	7.7841	22.3	1.768	H14
19.1	100.2	4.5	960	1.01	15.2	7.7841	22.3	1.768	H14

19.1	100.2	4.5	864	1.01	15.2	6.3051	22.3	1.768	H14
19	97.02	4	672	1.01	13.8	4.4794	24.3	1.872	H15
19	97.02	4	608	1.01	13.8	3.6668	24.3	1.872	H15
19	97.02	4	608	1.01	13.8	3.6668	24.3	1.872	H15
19	100.3	4.02	832	1.01	14.8	8.0342	25	1.937	H16
19	100.3	4.02	864	1.01	14.8	8.6641	25	1.937	H16
19	100.3	4.02	800	1.01	14.8	7.4281	25	1.937	H16
18.9	96.31	3.95	800	1.01	14.1	6.6162	24.4	1.959	H17
18.9	96.31	3.95	800	1.01	14.1	6.6162	24.4	1.959	H17
18.9	96.31	3.95	768	1.01	14.1	6.0974	24.4	1.959	H17
19	96.16	3.85	864	1.01	13.2	7.7291	25	1.877	H18
19	96.16	3.85	768	1.01	13.2	6.107	25	1.877	H18
19	96.16	3.85	960	1.01	13.2	9.5421	25	1.877	H18
21.5	130.2	6.13	1888	1.01	133	202.42	21.2	7.742	a-36
25.6	100.6	5.03	4864	1.02	49.9	354.41	20	3.859	alumina
20.1	130.3	6.35	1856	1.02	45.4	64.586	20.5	2.725	aluminum

Table 3. Foundry M Results for Young's Modulus and Strength

Sample	Strength (Pascals)	Elastic Modulus(GPa)
1_1	10916179.34	5.114198755
2_2	12354209.3	4.894737722
2_3	13502565.49	5.085859171
2_4	10924663.52	1.938240207
3_1	11774092.37	2.341366459
3_2	14690179.11	2.978673175
3_3	16195233.54	3.569169751
3_5	13634380.45	3.782327428

Table 4 -- Foundry H Results for Strength and Young's Modulus

Sample	Elastic Modulus (GPa)	Strength (MPa)
H1	7.114754	3.80108
H5	8.768534	2.713753
H6	6.361932	3.112619
H9	7.464192	3.694802
H13	8.771506	2.635552
H14	7.291106	3.378315
H15	3.937699	2.988031
H16	8.042135	3.372148
H17	6.44325	2.56
H18	7.792731	2.749888

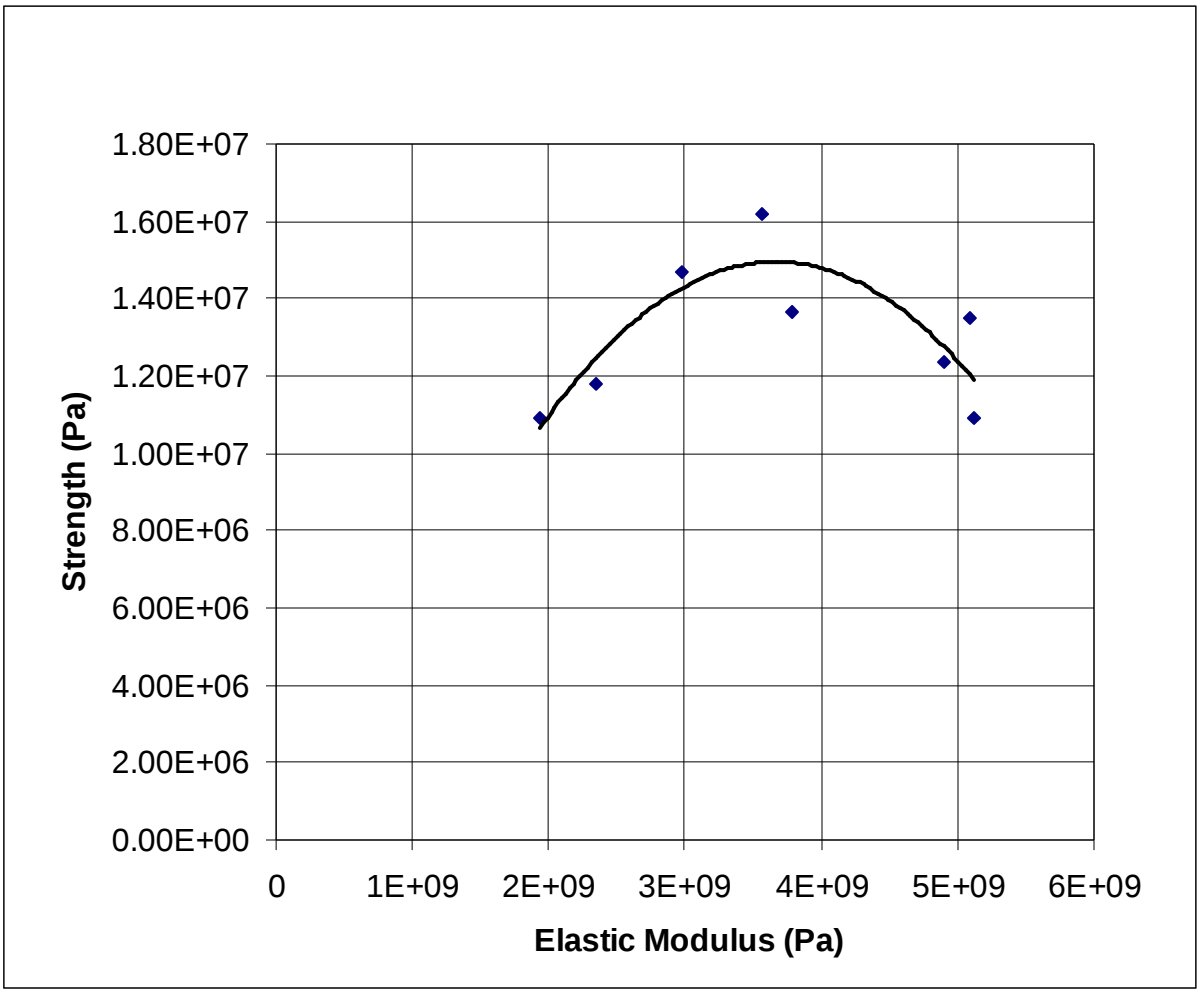

Figure 1 -- Foundry M: Strength vs. Elastic Modulus

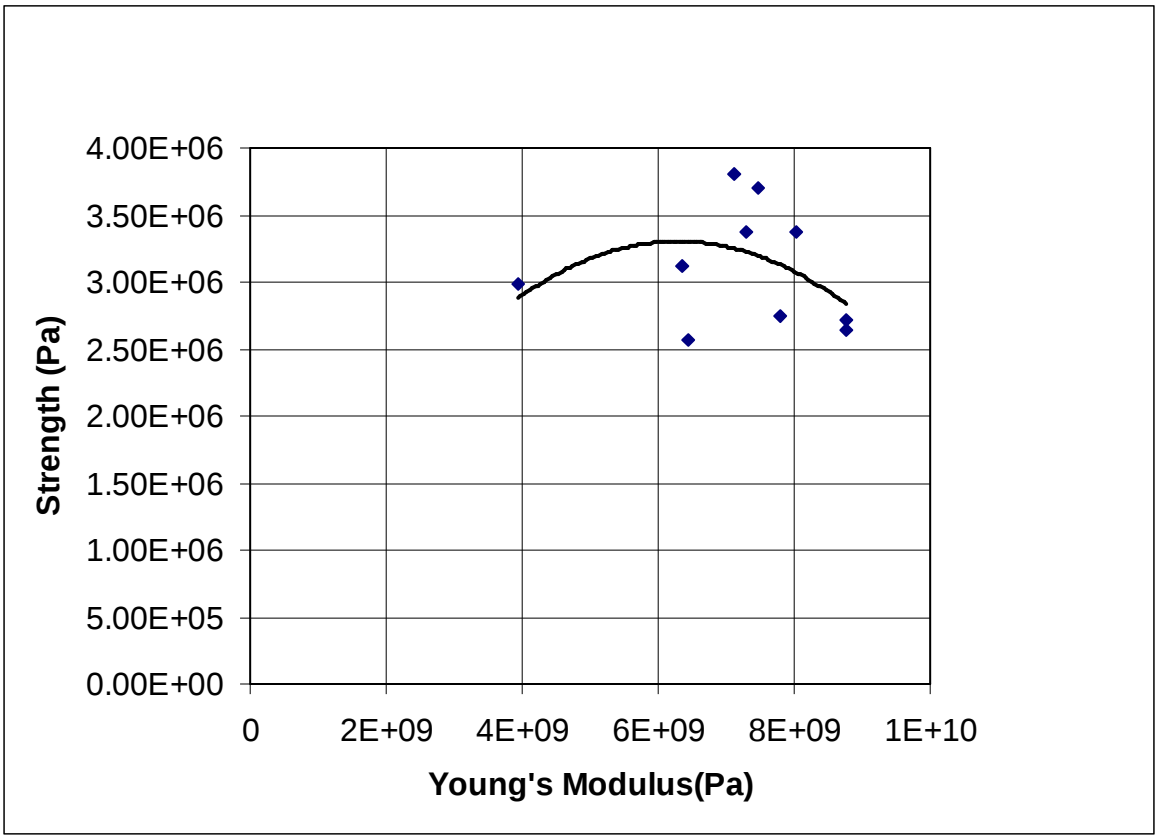

Figure 2 Foundry H: Strength vs. Young's Modulus

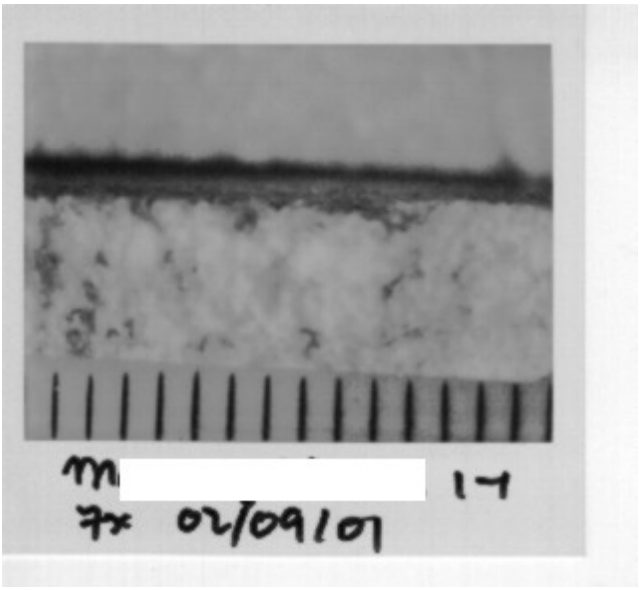

Figure 3a -Foundry M 1_1 bar. (Scale increments are 1 mm)

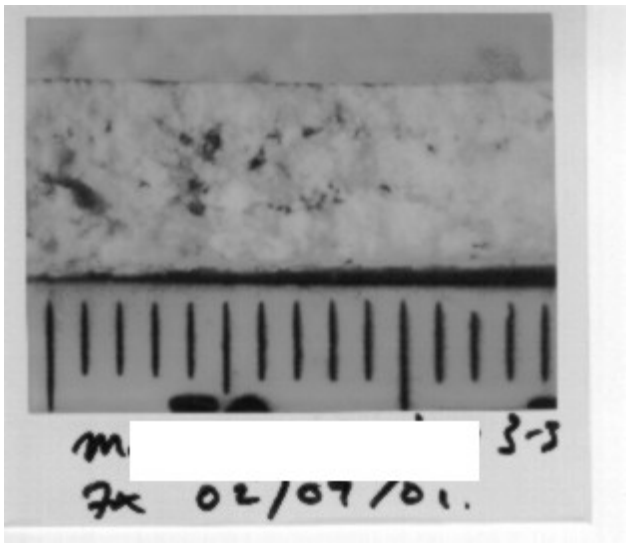

Figure 3b -- Foundry M 3_3 bar (scale increments are 1 mm)

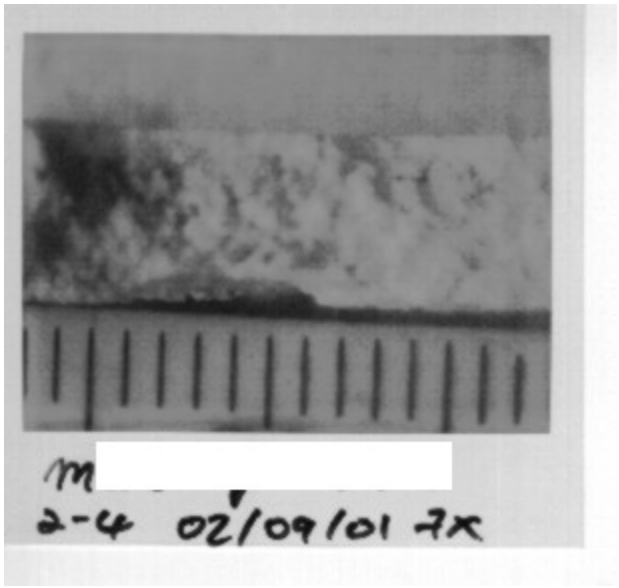

Figure 3c -- Foundry M 2_4 bar (scale increments are 1 mm)

VII. STATISTICAL ANALYSIS OF THREE-POINT AND FOUR-POINT BEND TESTING FOR THE CHARACTERIZATION OF CERAMIC MOLD SHELLS

Student Participants; Sony Mascreen, Phil Jackson

And

Dr.Von L. Richards, Ph.D.

University of Missouri at Rolla

VII.(i) Introduction:

The objective of our program was to examine measurements that could be used to characterize variability in the process that relates to the frequency of shell cracking. The four-point bend method puts more sample volume of material under uniform stress. This facilitates finding the critical flaw that may be randomly placed in the sample as a consequence of process variability. In the earlier section (section II) it was explained that the molded test bar is more representative of the shell building process than a sanded or sawed bar prepared from a flat sample and the four-point bend method should be more representative of the weakest link in the shell structure. But it was not been proven to a statistically significant extent. A two-way ANOVA with replication (which looks into the possibility of interaction) is used to compare the two bend tests and the two sample types to reach a statistical conclusion. The two factors used here are, one is the specimen condition and the second is the type of bend test. The two types of specimen conditions are molded test specimen and sawed test specimen. The preparation for which will be explained later in this section.

VII.(ii) Sample Preparation:

The ceramic test bars used in this procedure were made with the tensile side against the wax. Figure 1 shows the wax mold for the test specimen. The mold then went through the shell build process used by Pittsburg State University. The tensile bar thus produced has a flattened “U” shape to it as shown in figure 2. The samples for these tests were made in Pittsburg State University. Two types of sample where used from the same shell. One is the molded sample and the other sawed sample.

VII.(ii).a. Molded Samples:

The bars were produced by Pittsburg State University using the mold designed for producing four point bend test bars. Fired bar material was used for the processes described here. The test bars would be cut on the compression side (rough side). Nothing was done to the tensile (smooth) side. Using the diamond saw, the bar was cut on the compression side to remove the legs of the "U" until a flat specimen remained. A 260-grit diamond-polishing wheel was used to obtain the desired flat surface. Once the specimens were ready, they were heated in an oven at 150°C for three hours to dry them. Length and thickness were measured in millimeters and recorded. The samples were then broken on the bending apparatus shown in figure 3.

VII.(ii).b. Sawed Samples:

The sawed samples are cut out from the back shell that we have after cutting the molded samples. The dimensions of the sawed sample are kept as close to that of the molded sample so that there is no any statistical errors due to dimensional discrepancies. Also each sawed sample is identified with the molded sample in terms of the similar shell from which both were sawed. Fired bar material was used for the processes described here. The tensile sides of the bar were affected when we cut the specimen. Using the diamond saw, the bar was cut on the compression side to get the rough shape. A 260-grit diamond-polishing wheel was used to obtain the desired dimensions. Once the specimens were ready, they were heated in an oven at 150°C for three hours to dry them. Length and thickness were measured in millimeters and recorded.

VII.(iii) Experimental Procedure:

The samples are carefully sorted out and grouped together in batches of molded and sawed samples. The four point and three point bend tests were conducted. The breaking strength of the samples was calculated in MPa. An analysis of variance (ANOVA) was done for two-factor replication. The two factors taken into account are the bend testing and the specimen conditions.

VII.(iv) ANOVA Two-Factor with Replication:

An ANOVA analysis for two-factor replication was done on the data obtained. The two-way analysis of variance with replication deals with the case where two different

experimental factors have been studied simultaneously. For each factor, it tests whether the differences resulting from the various levels are statistically significant. It also tests for any interaction between the two factors - i.e. does some combination of treatments produce a special effect that could not be accounted for as the simple sum of the two factors acting separately.

VII.(v)Results:

The statistical analyses of the tests done are show below. Table 1 shows ANOVA table for two-factor replication. These results are got using Stat Graphics, a statistical data analysis tool. Figures 6 and 7 show the scatter plot of the two factors i.e. Test type and specimen condition. Figure 8 and 9 shows the mean and 95 % confidence intervals of the two factors explored and figure 10 shows the interaction between them and the 95% confidence interval.

VII.(vi) Discussion of Results:

The ANOVA for two-factor replication done on the three-point and four-point bend test with different specimen conditions are shown in table 1. The sample size used is 128 samples each for both the tests and a total of 256 samples were used as for this analysis. The ANOVA table decomposes the variability of result into contributions due to various factors. The P-values test the statistical significance of each of the factors. The first factor chosen was the test type. Since the P value is less than 0.05, the test type (4-point and 3-point) has a significant effect on result at the 95% confidence level. The second factor was the specimen condition, molded or sawed specimen, for this factor the P value is less than 0.05, and so the specimen condition has a significant effect on the result at 95% confidence level. Now we see the interaction between the two factors. The P values for the interaction of two factors is less than 0.05, hence the two factors show a significant interaction on the result at 95% confidence interval.

Figure 3 and 4 shows the scatter plot of the test types and the specimen conditions respectively. Figure 3 shows that the three-point bend test is more scattered than the four-point bend test. The scatter plot suggests that four-point bend test is more appropriate to estimate the mean strength of a population because the variation of the

strength in the sample population is low whereas three-point bend test shows a large variation of strength, which in turn will affect the population mean of the sample. Figure 4 shows the scatter plot for the specimen conditions that is the molded and sawed specimens. The scatter plot doesn't show a big scatter in either of the specimen condition other than a single flyer in the sawed sample. One of the important things to keep in mind while examining a scatter plot is that it is just gives a basic idea of the scattering of results. One cannot come to any statistical conclusions just based on scatter plot. Figures 5 and 6 shows the further exploration of results in terms of mean and the 95% confidence intervals. Figure 5 shows that the three-point bend test gives a higher mean for the same samples. A logical explanation for this trend to higher mean strengths in the three point bend test as compared to the four point bend test is that a smaller region of the sample is exposed to the maximum tensile stress in the three point bend test than in the four point test. Thus, the probability of encountering a flaw from the large size tail of the population distribution is lessened when three-point bend is used. The comparison of mean and 95% confidence intervals of molded and sawed samples are shown figure 7. Here the molded samples show a lower mean strength and the sawed samples seem to have higher mean strength. This trend can be attributed to the breaking of the weak bars during sanding operation on the sawed samples to obtain straight edges on the test bars from flat coupons. Thus the weaker bars from the sample population were eliminated, giving a false high mean strength. At the same time, the sawing and sanding introduced flaws in the edge of the test pieces on the tensile side, which superimposed another flaw distribution in addition to the flaws introduced in the shell-making process. This would give rise to the broadened breaking stress distribution compared to the proposed test article design. The molded bars did have clean-up diamond saw cutting and sanding on them to generate a uniform and measurable thickness, but this was all done on the compression side of the flexure bar, while the tension side and its edges were generated by the wax pattern.

The interaction between the two factors and the 95% confidence intervals of each factors are shown in figure 8. Here one can see that there is a significant interaction between the sample preparation and the bend tests. The decrease in the mean strength of the molded specimen from the three-point to the four-point bend test was higher (1.0

Mpa) when compared to sawed specimen (0.4 Mpa). This again emphasizes the fact that the sawed test specimen doesn't reveal the actual flaw population of the ceramic samples used. The sawing and sanding introduced flaws in the edge of the test pieces on the tensile side, which superimposed another flaw distribution in addition to the flaws introduced in the shell-making process. This gives a false higher mean strength in both the four-point and three-point testing method. The reason that there is a significant interaction can be attributed to the fact that three-point bend test gives a higher mean strength for the molded bar where as four-point bend test shows much lower strength. Since the tensile side of the bar was kept intact during machining and sanding of the test bar, the original flaw population is preserved. On a three-point bend test, only smaller portion of sample is exposed to maximum tensile strength, hiding the flaws outside that region, this gives a false higher mean strength for the samples.

VII.(vii) Conclusions and Recommendations

The conclusion we have reached after these statistical analyses are:

1. The molded test bar is more of a representative of the shell building process than a sanded or sawed bar prepared from a flat sample.
2. It is statistically proven that the four-point bend method should be more representative of the weakest link in the shell structure.
3. The mean strength of the population is dependent upon both the factors i.e. the test type and the sample condition on a 95% confidence level.

Recommendation:

To know the actual strength and affect of all the flaw population it is recommended to use a molded sample on a four-point bend test for the bend tests.

VII.(viii) Reference:

1. *Richards, Von L. and Connin, Ginger., "Four-Point Bend Testing to Characterize the Strength of Ceramic Mold Shells", Investment Casting Institute, 49th Annual Technical Meeting 2001, Paper No. 13, pg.13.1-13.10.*
2. *Baratta, Francis I., "Requirements for Flexure testing of Brittle Materials", AMMRC TR 82-20, Army Materials and Mechanics Research Center, Watertown, MA, 1982.*

Figure 1. Wax Test Mold

Figure 2. Tensile Side of the Molded Test Bar

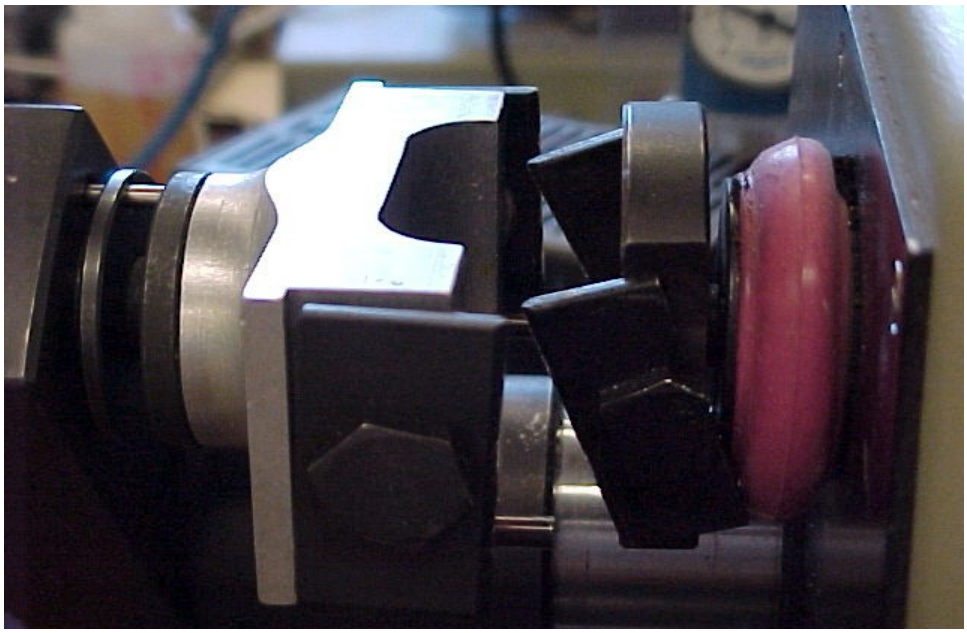

Figure 3. Bending Apparatus with a Four Point Fixture

Analysis of Variance for Two Factors with Replication					
Source	Sum of Squares	DF	Mean Squares	F-Ratio	P-Value
MAIN EFFECTS					
A: Test Type	34.65	1	34.65	44.22	0.0000
B: Specimen_condition	29.70	1	29.70	37.91	0.0000
INTERACTIONS					
AB	5.19	1	5.19	6.63	0.0106
RESIDUAL	197.45	252	0.78		
Total (Corrected)	266.99	255			

Table 1

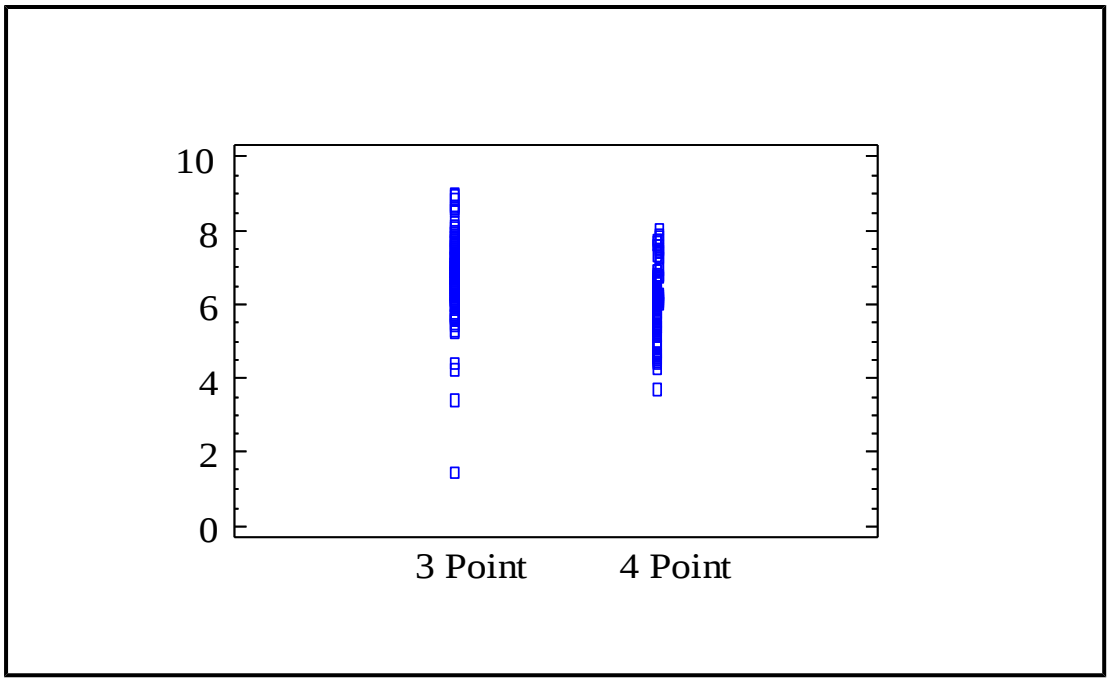

Figure 4. Scatter Plot for Test Type

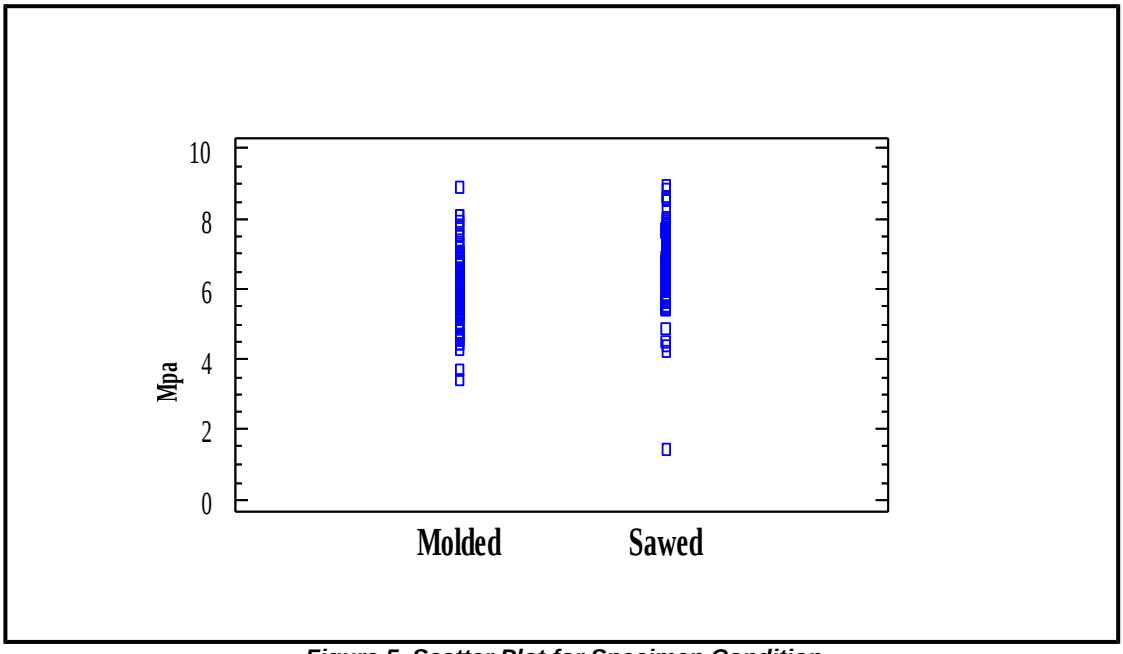

Figure 5. Scatter Plot for Specimen Condition

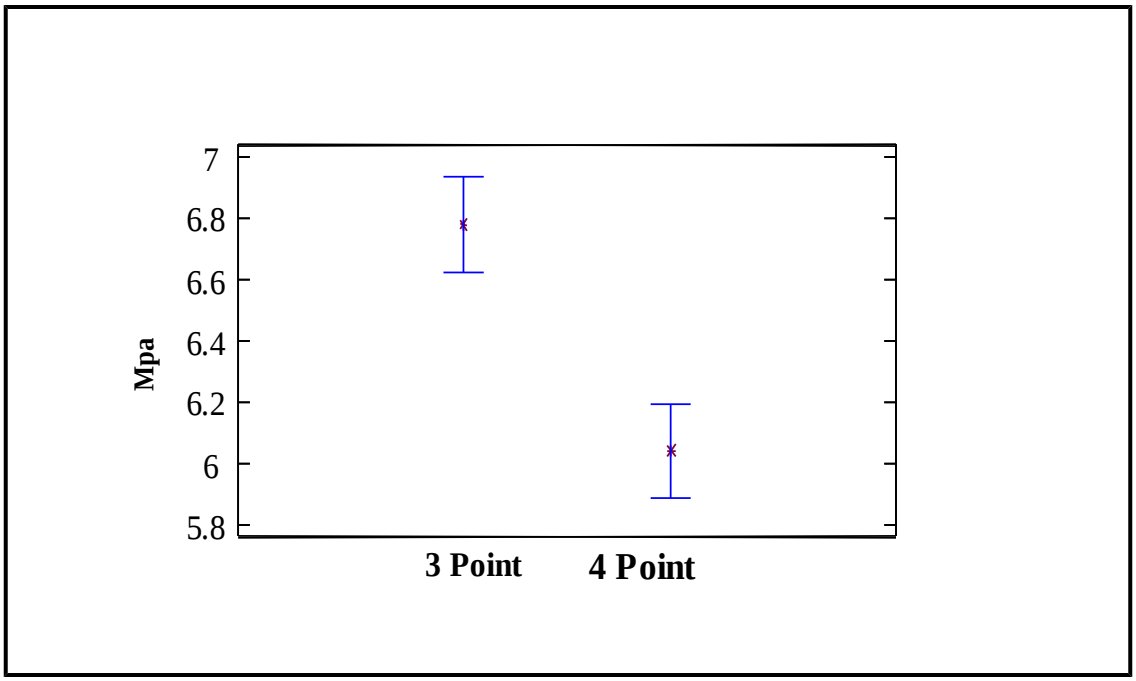

Figure 6. Mean And 95% Confidence Interval for Different Test Types

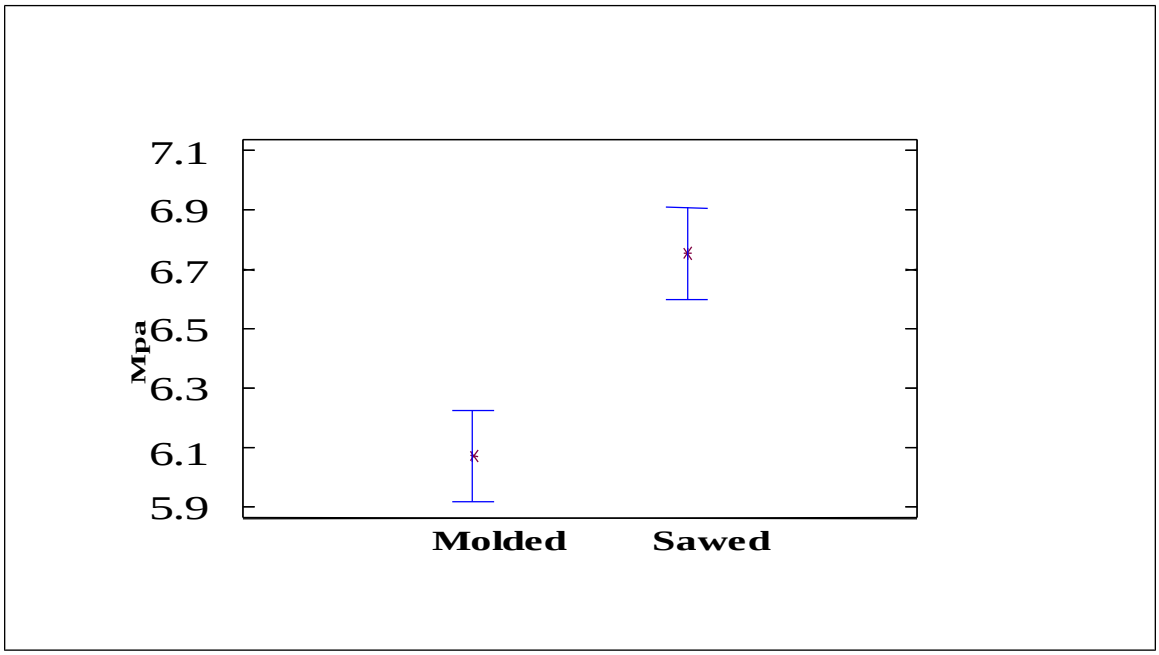

Figure 7. Mean And 95% Confidence Interval for Different Specimen Condition

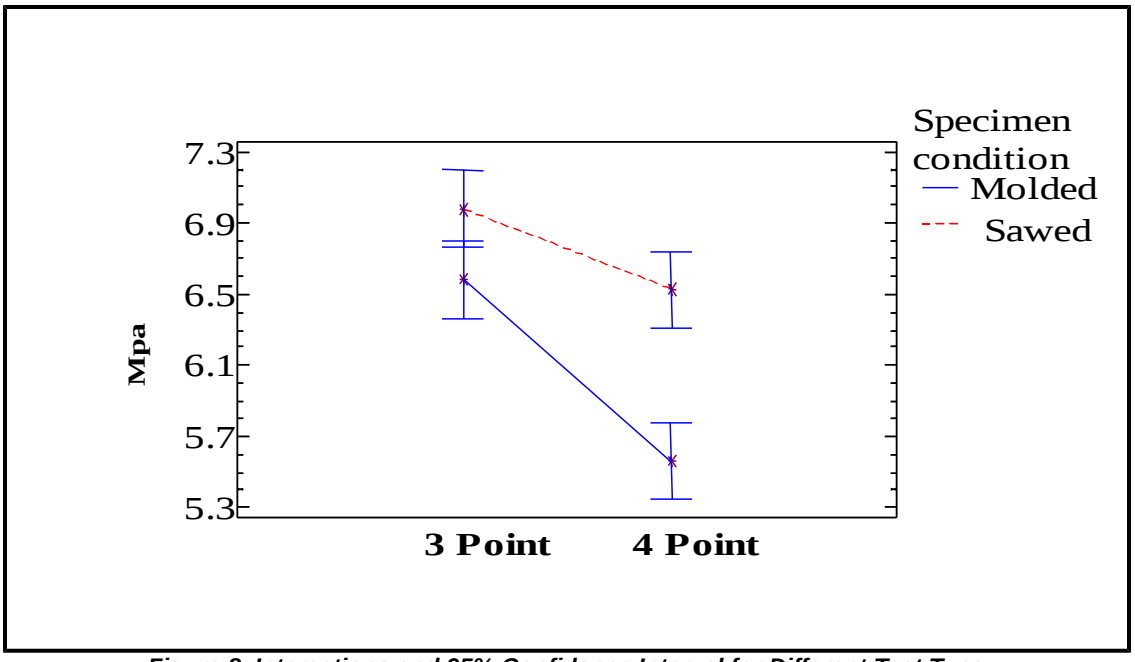

Figure 8. Interactions and 95% Confidence Interval for Different Test Type

VIII. THERMAL EXPANSION OF SHELL: A STUDY

VIII.(i) Introduction:

Thermal expansion of shell allows calculation of the free strain that can occur in shell systems. With this data and the properties of the wax, the superposition of strain method can be used to calculate the stress during critical steps of the investment casting process. The thermal expansion of the shell not only looks in to the volume expansion of shell on heat-up, but also the extent of sintering that can occur in the preheat furnace. In certain cases the stresses can occur as a result of temperature gradient between the inside and outside of the shell. These stresses can result in metal fining. The thermal expansion behavior of the shell can affect casting dimensions in another way besides the normal increase in size with temperature and sintering shrinkage. Shell cracks that occur during the autoclave or furnace pre-heat operations often result in metal fins on casting. The fins increase the distance between features perpendicular to the fin. They also cause the shell wall around the fin to bulge outward for an inch or two. This metal together with the fin must be removed by surface grinding.

VIII.(ii) Sample Preparation:

The sample for testing the thermal expansion is cut off from a broken test bar used for 4-point bend test by sawing and grinding. The dimensions are approximated to length equal to 1 inch, thickness of 0.15 inch and width of 0.2 inch. The sample is ground to have flat ends, so that it fits readily without any slipping in the dilatometer.

VIII.(iii) Procedure:

The sample dimensions were measured. An Orton’s Dilatometer measured the expansion of the shell material produced by participating foundries. The expansion temperature range was set between 50 C and 1000 C and the heating rate was 3C/min to the peak temperature. The cooling rate was also kept at 3C/min to the lowest temperature.

VIII.(iv) Results:

Figure 1 shows that the thermal expansion of participant A and C follows same pattern. The sintering shrinkage starts around 850C for both participants' material. No sintering shrinkage was observed in material from participant B. Figure 2 shows the standard material at foundry B and a special mix that contained polymer fiber. The plots of both materials from participant B overlap. This shows that the fugitive polymer fiber in the specimen seems to have no role in thermal expansion of shell.

VIII.(v) References:

1. *Snow, Jerry. D., and David Scott, "Prime Slurries for Investment Casting", Investment Casting Institute, 47th Annual Technical Meeting 1999, pg.6.1-6.21.*

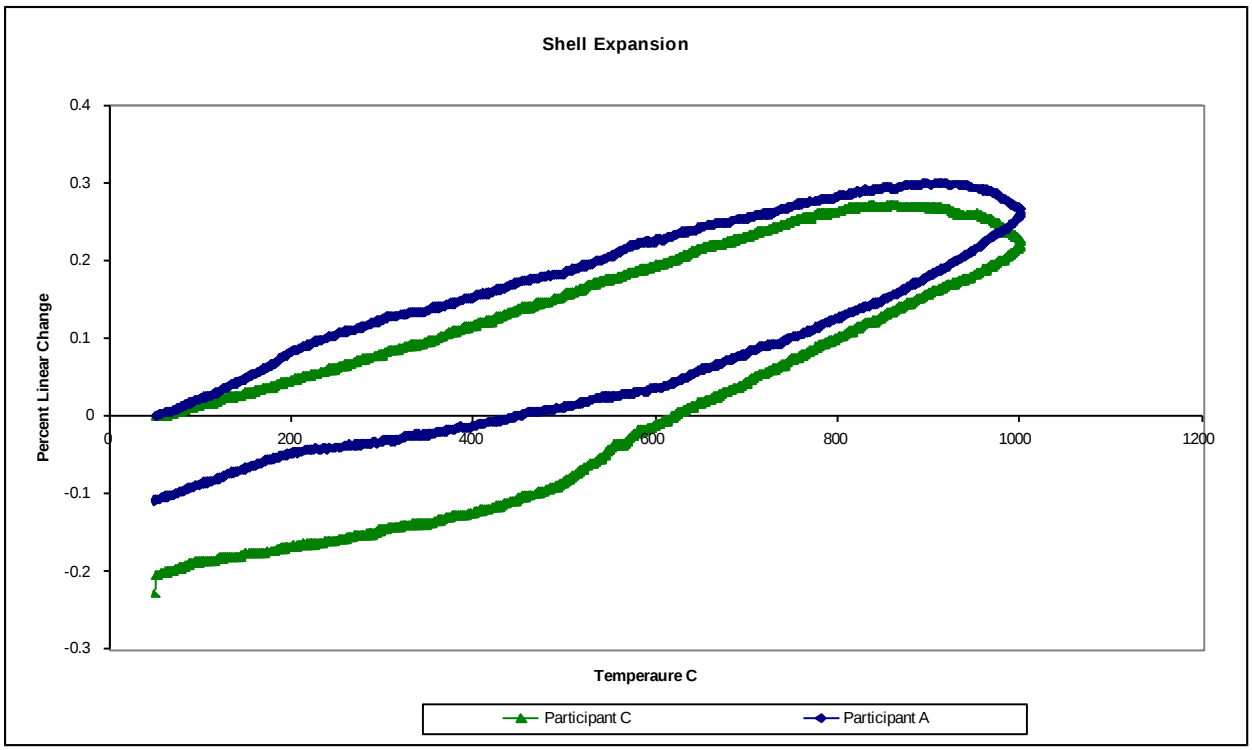

Figure 1: Comparison between Shell Expansions of Participant A with Participant C

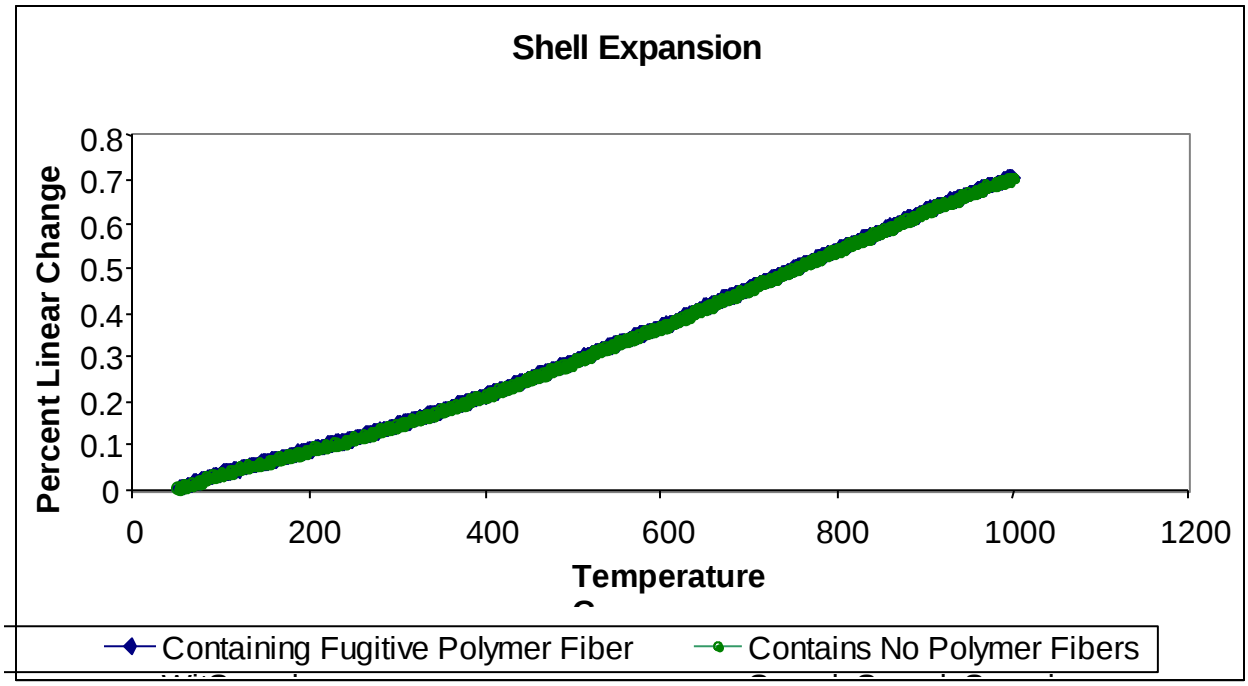

Figure 2: Comparison between Fired Shell Expansion of Materials that Contained Fugitive Polymer Fiber and Materials that did not Contain Fugitive Polymer Fiber from Participant B

IX. PERMEABILITY AND MICROSTRUCTURE ANALYSIS OF INVESTMENT CASTING SHELLS

By

Phillip Jackson (Student Participant)

University of Missouri – Rolla

And

Dr. Von Richards Ph.D.

University of Missouri – Rolla

IX.(i) Background

The concept behind performing a permeability analysis on investment casting shells is to determine the ability of the shell to relieve the stress accumulated by the creation, movement, and trapping of gasses during the auto-clave process. It is logical that the more permeable shell will provide a greater volume of gas to escape, and thereby help to reduce the total amount of stress provided against the shell. A secondary goal that developed in the course of experimentation was to test if the addition of a polymer fiber to the ceramic slurry increases the permeability of the sample. Previous work supported that this was true. In the course of work we produced results that supported the idea that the fibers actually reduced permeability.

For this experiment we used a series of samples created with the test bar mold for fracture toughness testing. The design of the experiment was to analyze the flow of air through a core sample of the ceramic material. Several participant foundries produced the shells used for the experiment. These foundries will be referred to as A, B, C. An analysis of results was used to compare the participant foundries. Foundry B was used to develop the work for the results of the secondary goal.

VIII.(ii) Results to Date

As a result of permeability testing we were better able to develop an understanding as to which methods of shell making are better suited to prevent cracking in the production process. Most foundries have a preferred selection of materials that are used to create the ceramic shells used for casting. The experiment designed for permeability produces a valid measure toward the choice of method for creating shells.

IX.(ii).a. Sample Selection and Preparation

Samples were collected from each of three participant foundries. Using the back plate from the fired shells created for fracture toughness analysis, a 0.5” core samples were drilled. The drilled samples were labeled in accordance with the foundry and shell. These samples were processed with a device to measure the pressure drop across the sample. (Figure 1). Using Darcy’s Law a specific permeability was determined for each sample and the average was taken for comparison.

IX.(ii).b. Foundry Results

The permeability tests run for the participant foundries resulted in a collaboration of results. Ten samples from foundry A were tested for permeability. Figure 2 shows results for specific permeability from these tests ranged from 2.391 E -12 m2 to 4.812 E –12 m2. The average result for the testing of samples containing polymers was 3.671 E –12 m2.

Foundry B participated with two types of shells. Ones referred to as NP do not contain the added polymer fibers in the slurry. Those referred to as A contained the fibers. Sixteen samples from category A were tested for permeability. (Figure 2) Results for specific permeability from these tests ranged from 8.053 E –13 m2 to 1.431 E –12 m2. The average result for the testing of samples containing polymers was 1.003 E –12 m2.

Fourteen samples from category NP were tested for permeability with results from these tests ranged from 7.415 E –12 m2 to 1.387 E - 11 m2. The average result for the NP test was 1.285 E –11 m2 viewable in figure 2.

Foundry C results were based off of fifteen samples that were tested for permeability. These results for specific permeability ranged from 8.57 E -13 m2 to 1.67 E –12 m2. The average result for the testing of samples 1.243 E –12 m2 as show in figure 2.

A comparison was done between each of the three participants. Students T test was used to calculate the probability that samples from one source would fall into the specific permeability range of another location. In all cases the T test stated that 99.99% of the samples from any given foundry would fall in the range of another. A clear

distinction can be made of the non-fibrous samples from foundry B. This high permeability rate suggests that the slurry material and preparation method are preferable to improve the permeability of shells.

IX.(ii).c. Polymer Fiber versus Non – Fiber samples

A comparison was done between the previously mentioned samples A and NP from participant foundry B. Figure 3 shows clearly a large difference in permeability between the sample types. Figure 3 also shows that the measured permeability in all cases was significantly higher in the non-fibrous samples. This suggests that the NP samples would perform much greater in the dispersion of gasses. However, in congruence with fracture toughness (Section III), the results do not suggest an overall increase in performance of the ceramic shells.

IX. (ii).d. Microstructure

Some research was done with the microstructures of the permeability samples. The set up included microscope pictures using a light microscope with camera attachment. The concept was to use point and line count measurements to obtain a volume to surface area ratios. The initial pictures were taken and the prime coat as the assumption was made that this coat provided the limiting factor for the permeability of the sample. Several problems were encountered with this process. Mostly due to the inability to produce pictures with clear distinctions between mounting material and ceramic matrix, the results were limited namely to qualitative analysis. No conclusive evidence has yet been obtained from this micro-picture study. Figures 4 and 5 show examples of the microstructures.

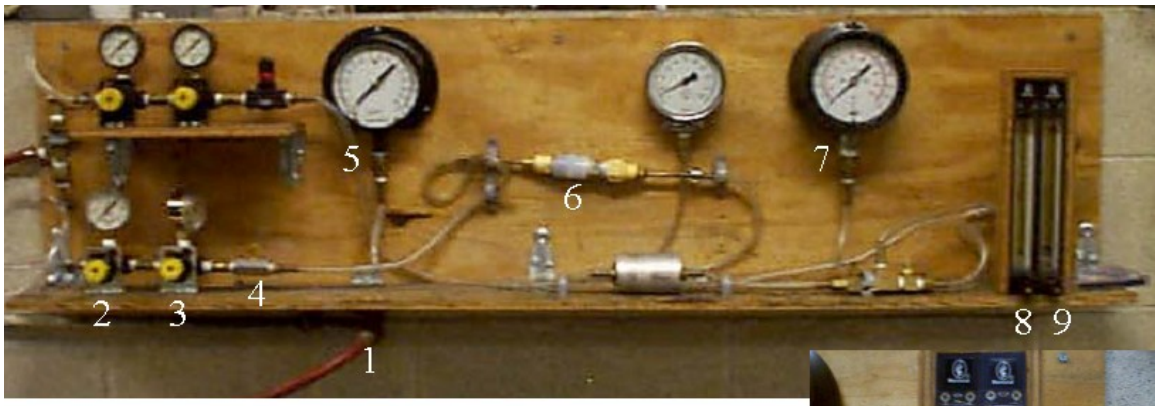

1. Main Air Supply Valve
2. Control Valve 1
3. Control Valve 2
4. Stop Valve
5. Inlet Pressure
6. Sample Chamber
7. Outlet Pressure
8. Flow Gauge 1

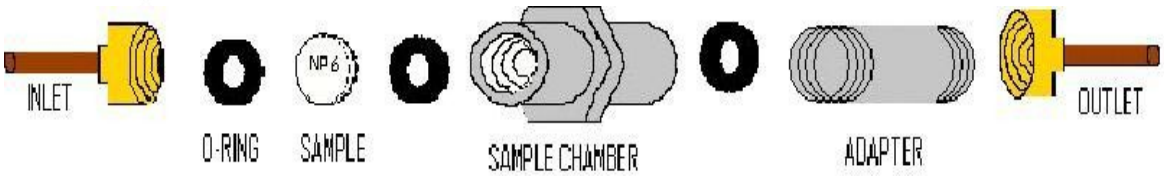

Figure. 1

Foundry A vs. Foundries C and B

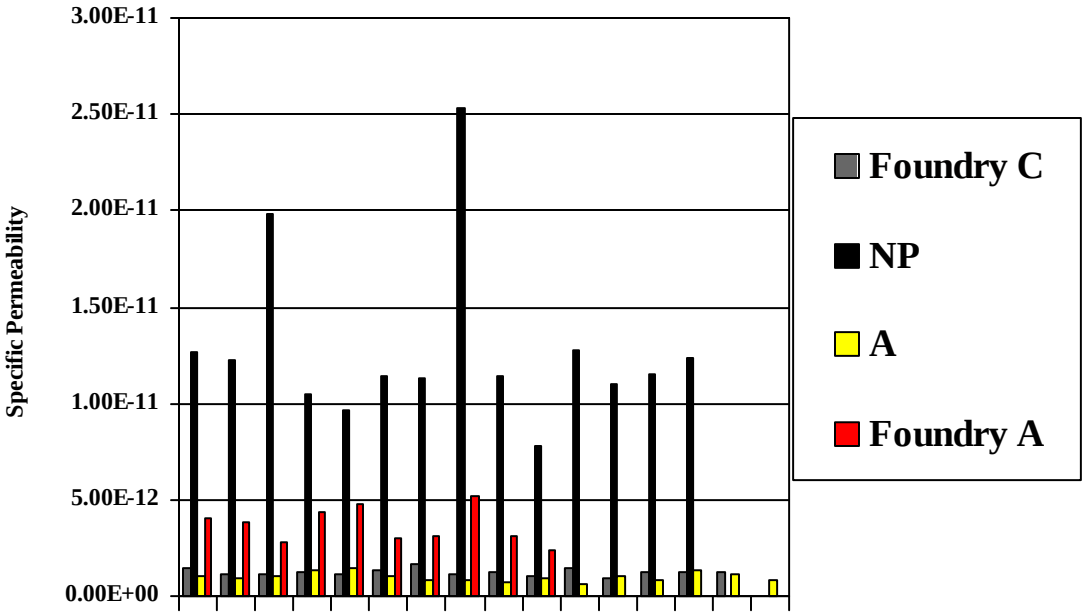

Figure 2

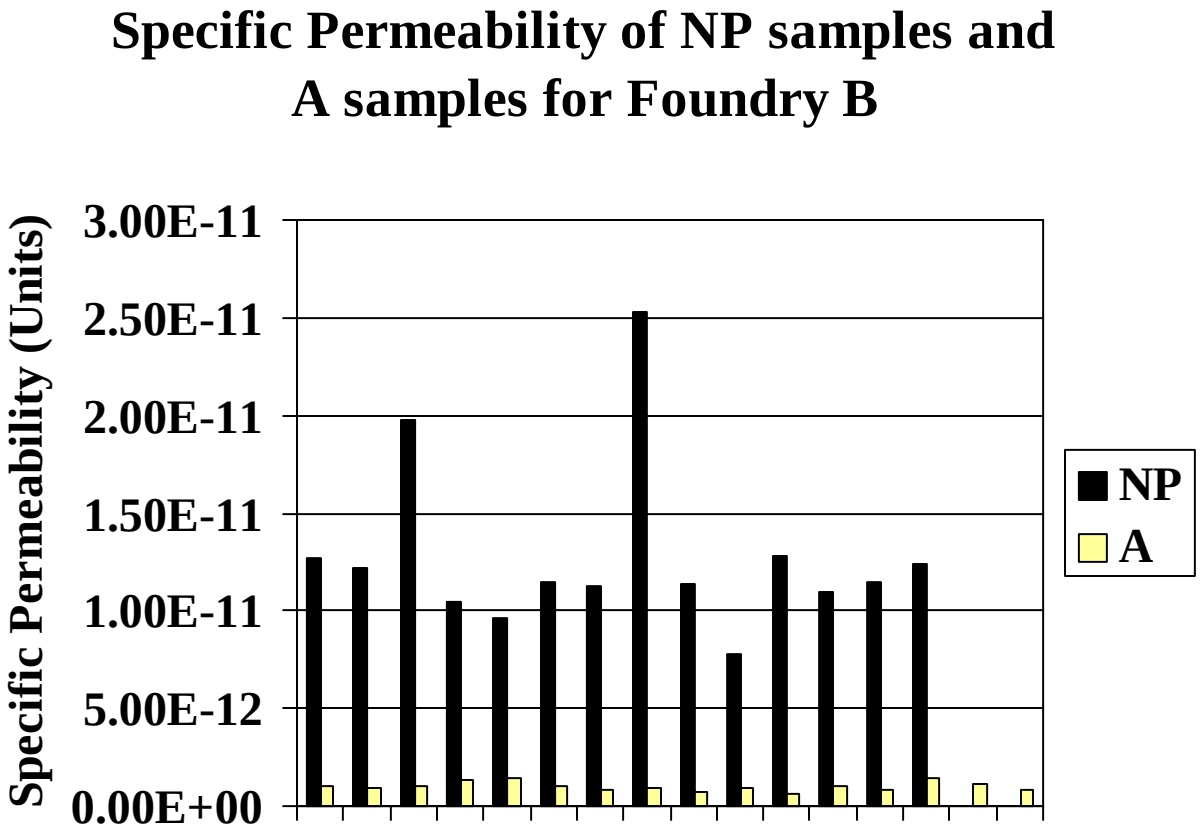
Specific Permeability of NP samples and A samples for Foundry B
Specific Permeability (Units)
3.00E-11
2.50E-11
2.00E-11
1.50E-11
1.00E-11
5.00E-12
0.00E+00
NP
A

Figure 3

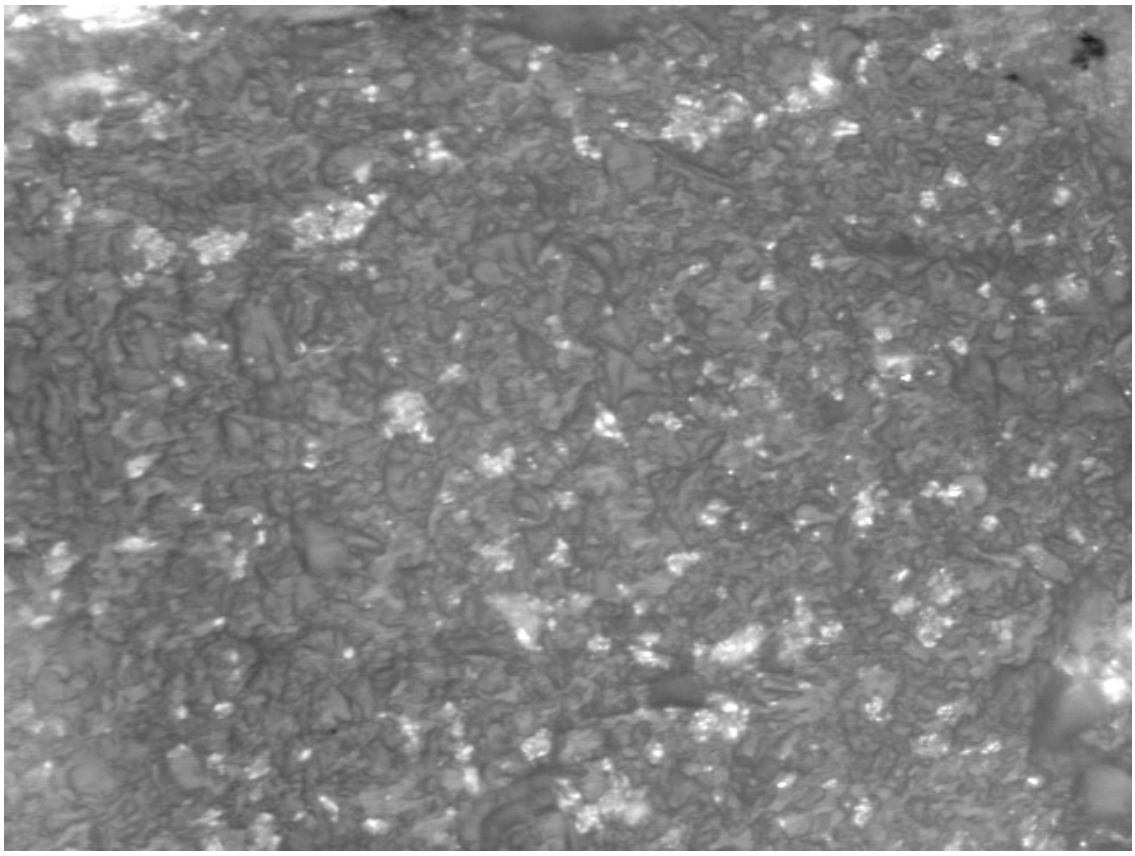

Figure 4: NP22 at 50X

NP22 at 50X

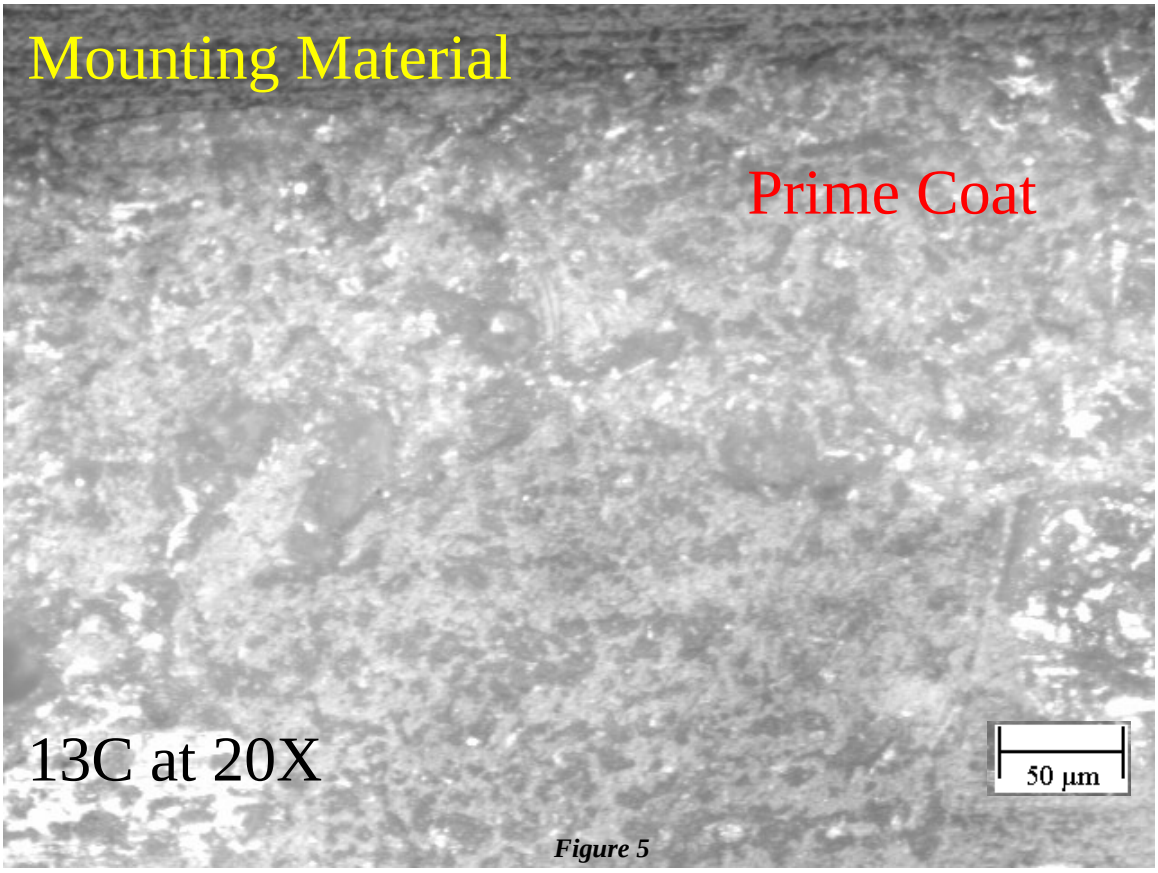

Figure 5

X. List of Papers Published

(1) Four Point Bend Testing to Characterize the Strength of Ceramic Mold Shells, Von L. Richards and Ginger Connin, Investment Casting Institute 49th Annual Meeting and Exposition paper number 13, 2001.

(2) Thermal Expansion of Investment Casting Pattern Wax, Brian V. Sunderland and Von L. Richards, Investment Casting Institute 49th Annual Meeting and Exposition paper number 2, 2001.

(3) Investment Casting Shell Cracking, Von L.Richards, Deepak Rasquinha, and Brian Sunderland, Steel Founder's Society Technical and Operating Conference Proceedings November 2001.

(4) Four-point Bend Testing Method More Accurately Characterizes Strength of Ceramic Mold Shells, Von L. Richards, and Ginger Connin, INCAST, April 2002, pp. 22-25.

(5) Thermal Expansion of Investment Casting Pattern Wax, Von L. Richards and Sony Mascreen, AFS Transactions, 2003, paper number 03-040 accepted for publication._

(6) Fracture Toughness of Investment Casting Shells Using Fractography, Von L. Richards and Sony Mascreen, Investment Casting Institute 50th Technical Conference and Expo, paper number 13, September 2002.

(7) Statistical Analysis of Three-point and Four-Point Bend Testing for the Characterization of Ceramic Mold Shells, Von L. Richards, Sony Mascreen, Phillip Jackson, and Thomas Hahn, Investment Casting Institute 51st Technical Conference and Expo, Paper Number 8, 2003.